Journal of Sound and Vibration (1999) **225**(5), 935–988
Article No. jsvi.1999.2257, available online at http://www.idealibrary.com on IDEAL®

DYNAMICS OF TRANSVERSELY VIBRATING BEAMS USING FOUR ENGINEERING THEORIES

SEON M. HAN, HAYM BENAROYA AND TIMOTHY WEI

Mechanical and Aerospace Engineering, Rutgers, the State University of New Jersey, Piscataway, NJ 08854, *U.S.A.*

(*Received* 18 *September* 1998, *and in final form* 22 *March* 1999)

In this paper, the full development and analysis of four models for the transversely vibrating uniform beam are presented. The four theories are the Euler–Bernoulli, Rayleigh, shear and Timoshenko. First, a brief history of the development of each beam model is presented. Second, the equation of motion for each model, and the expressions for boundary conditions are obtained using Hamilton's variational principle. Third, the frequency equations are obtained for four sets of end conditions: free–free, clamped–clamped, hinged–hinged and clamped–free. The roots of the frequency equations are presented in terms of normalized wave numbers. The normalized wave numbers for the other six sets of end conditions are obtained using the analysis of symmetric and antisymmetric modes. Fourth, the orthogonality conditions of the eigenfunctions or mode shape and the procedure to obtain the forced response using the method of *eigenfunction expansion* is presented. Finally, a numerical example is shown for a non-slender beam to signify the differences among the four beam models.

1. INTRODUCTION

The beam theories that we consider here were all introduced by 1921. That is, the problem of the transversely vibrating beam was formulated in terms of the partial differential equation of motion, an external forcing function, boundary conditions and initial conditions. Many efforts had been devoted to obtaining and to understanding the solution of this non-homogeneous initial-boundary-value problem. However, work on this subject was done in a patchwork fashion by showing parts of the solution at a time, and there is no paper that presents the complete solution from the formulation of the governing differential equation to its solution for all four models. The most complete study was done by Traill-Nash and Collar [1], but they only derived the frequency equations for various end conditions for four models. In this paper, the partial differential equation of motion for each model is solved in full obtaining the frequency equations for each end condition, the solutions of these frequency equations in terms of dimensionless wave numbers, the orthogonality conditions among the eigenfunctions, and the procedure to obtain the full solution to the non-homogeneous initial-boundary-value problem using the method of *eigenfunction expansion.*

0022-460X/99/350935 + 54 $30.00/0

For engineering purposes, the dimensionless wave numbers are tabulated or plotted as functions of the slenderness ratio so that the natural frequencies can be obtained directly for given geometrical and physical properties. The comparisons among the natural frequencies and the dimensionless wave numbers of the four models are then made. It is shown that the differences between the the Euler–Bernoulli model and the other models monotonically decreases with increasing slenderness ratio defined by the ratio of length of the beam to the radius of gyration of the cross-section. A numerical example is given for the case of a non-slender beam so that the differences among models are noticeable.

Following is a brief history of the development of each beam model.

1.1. LITERATURE REVIEW

An exact formulation of the beam problem was first investigated in terms of general elasticity equations by Pochhammer (1876) and Chree (1889) [2]. They derived the equations that describe a vibrating solid cylinder. However, it is not practical to solve the full problem because it yields more information than usually needed in applications. Therefore, approximate solutions for transverse displacement are sufficient. The beam theories under consideration all yield the transverse displacement as a solution.

It was recognized by the early researchers that the bending effect is the single most important factor in a transversely vibrating beam. The Euler–Bernoulli model includes the strain energy due to the bending and the kinetic energy due to the lateral displacement. The Euler–Bernoulli model dates back to the 18th century. Jacob Bernoulli (1654–1705) first discovered that the curvature of an elastic beam at any point is proportional to the bending moment at that point. Daniel Bernoulli (1700–1782), nephew of Jacob, was the first one who formulated the differential equation of motion of a vibrating beam. Later, Jacob Bernoulli's theory was accepted by Leonhard Euler (1707–1783) in his investigation of the shape of elastic beams under various loading conditions. Many advances on the elastic curves were made by Euler [3]. The Euler–Bernoulli beam theory, sometimes called the classical beam theory, Euler beam theory, Bernoulli beam theory, or Bernoulli–Euler beam theory, is the most commonly used because it is simple and provides reasonable engineering approximations for many problems. However, the Euler–Bernoulli model tends to slightly overestimate the natural frequencies. This problem is exacerbated for the natural frequencies of the higher modes. Also, the prediction is better for slender beams than non-slender beams.

The Rayleigh beam theory (1877) [4] provides a marginal improvement on the Euler–Bernoulli theory by including the effect of rotation of the cross-section. As a result, it partially corrects the overestimation of natural frequencies in the Euler–Bernoulli model. However, the natural frequencies are still overestimated. Early investigators include Davies (1937) [5], who studied the effect of rotary inertia on a fixed-free beam.

The shear model adds shear distortion to the Euler–Bernoulli model. It should be noted that this is different from the pure shear model which includes the shear

distortion and rotary inertia only or the simple shear beam which includes the shear distortion and lateral displacement only [6]. Neither the pure shear nor the simple shear model fits our purpose of obtaining an improved model to the Euler–Bernoulli model because both exclude the most important factor, the bending effect. By adding shear distortion to the Euler–Bernoulli beam, the estimate of the natural frequencies improves considerably.

Timoshenko (1921, 1922) [7, 8] proposed a beam theory which adds the effect of shear as well as the effect of rotation to the Euler–Bernoulli beam. The Timoshenko model is a major improvement for non-slender beams and for high-frequency responses where shear or rotary effects are not negligible. Following Timoshenko, several authors have obtained the frequency equations and the mode shapes for various boundary conditions. Some are Kruszewski (1949) [9], Traill-Nash and Collar (1953) [1], Dolph (1954) [10], and Huang (1961) [11].

Kruszewski obtained the first three antisymmetric modes of a cantilever beam, and three antisymmetric and symmetric modes of a free–free beam.

Traill-Nash and Collar gave a fairly complete theoretical treatment as well as experimental results for the case of a uniform beam. In the first part of their paper, they obtained the expressions for the frequency equation and mode shapes for six common boundary conditions: fixed–free, free–free, hinged–free, hinged–hinged, fixed–fixed and fixed–hinged. In the second part of the paper, they reported the experimental results with the numerical results obtained by the Euler–Bernoulli, shear, and Timoshenko models. They used non-slender beams in which the shear and rotary effects were important. They reported the difference for the first and second natural frequencies predicted by each of the theoretical models and the experimental values. The summary of the result is shown in Table 1.

Huang (1961) independently obtained the frequency equations and expressions for the mode shapes for all six end conditions. The frequency equations are difficult to solve except for the case of a simply supported beam. Even when the roots of the frequency equations are obtained, it is a challenge to present them in a meaningful way. For example, Traill-Nash and Collar (1953), Dolph (1954), Huang (1961) and Abbas and Thomas (1977) presented them in different ways.

Kruszewski, Traill-Nash and Collar, and Huang only gave expressions for the natural frequencies and mode shapes. They did not solve for the complete response

TABLE 1

The percentage deviates from the experimental values obtained by Traill-Nash and Collar (1953)

Beam models	First natural frequency	Second natural frequency
Euler–Bernoulli	+14% to +26%	+78% to +133%
Shear	0% to +3%	−1% to +6%
Timoshenko	−1% to +2%	−1% to +6%

of the beam due to initial conditions and external forces. To do so, knowledge of the orthogonality conditions among the eigenfunctions is required. The orthogonality conditions for the Timoshenko beam were independently noted by Dolph (1954) and Herrmann (1955) [12]. Dolph solved the initial and boundary-value problem for a hinged–hinged beam with no external forces. The methods used to solve for the forced initial-boundary-value problem and for the problem with time-dependent boundary conditions are briefly mentioned in his paper. A general method to solve for the response of a Timoshenko beam due to initial conditions and the external forces is given in the book *Elastokinetics* by Reismann and Pawlik (1974) [13]. They used the method of *eigenfunction expansion.*

A crucial parameter in Timoshenko beam theory is the shape factor. It is also called the shear coefficient or the area reduction factor. This parameter arises because the shear is not constant over the cross-section. The shape factor is a function of Poisson's ratio and the frequency of vibration as well as the shape of the cross-section. Typically, the functional dependence on frequency is ignored. Davies (1948) [5], Mindlin and Deresiewicz (1954) [14], Cowper (1966) [15] and Spence and Seldin (1970) [16] suggested methods to calculate the shape factor as a function of the shape of the cross-section and Poisson's ratio. Stephen (1978) [17] showed variation in the shape factor with frequency.

Despite current efforts (Levinson (1979, 1981) [18–20] to come up with a new and better beam theory, the Euler–Bernoulli and Timoshenko beam theories are still widely used.

A summary of the four beam theories is tabulated in Table 2. The basic assumptions made by all models are as follows.

1. One dimension (axial direction) is considerably larger than the other two.
2. The material is linear elastic (Hookean).
3. The Poisson effect is neglected.
4. The cross-sectional area is symmetric so that the neutral and centroidal axes coincide.
5. Planes perpendicular to the neutral axis remain perpendicular after deformation.
6. The angle of rotation is small so that the small angle assumption can be used.

TABLE 2

Four beam theories

Beam models	Bending moment	Lateral displacement	Shear deformation	Rotary inertia
Euler–Bernoulli	✓	✓	×	×
Rayleigh	✓	✓	×	✓
Shear	✓	✓	✓	×
Timoshenko	✓	✓	✓	✓

2. EQUATION OF MOTION AND BOUNDARY CONDITIONS VIA HAMILTON'S PRINCIPLE

2.1. THE EULER–BERNOULLI BEAM MODEL

Detailed derivations for the Euler–Bernoulli model can be found in text books by Benaroya [21], Inman [22], Meirovitch [23–25], Rao [26] and Thomson [27]. Here, the equation of motion is obtained using Hamilton's variational principle. The potential energy of a uniform beam due to bending is given by

$$PE^*_{bending} = \frac{1}{2}\int_0^{L^*} E^*I^* \left(\frac{\partial^2 v^*(x^*,t^*)}{\partial x^{*2}}\right)^2 \mathrm{d}x^*, \tag{1}$$

where E^* is the modulus of elasticity, I^* the area moment of inertia of the cross-section about the neutral axis, $v^*(x^*,t^*)$ the transverse deflection at the axial location x^* and time t^*, and L^* the length of the beam. Superscript $*$ symbols are used to signify that they are dimensional quantities. Now, the length scales (L^*, v^*, and x^*) are non-dimensionalized by the length of the beam so that dimensionless quantities (L, v, and x) are given by

$$L = L^*/L^* = 1, \qquad v = v^*/L^*, \qquad x = x^*/L^*. \tag{2}$$

In terms of the dimensionless length scales, the potential energy is given by

$$PE^*_{bending} = \frac{1}{2}\int_0^1 \frac{E^*I^*}{L^*}\left(\frac{\partial^2 v(x,t)}{\partial x^2}\right)^2 \mathrm{d}x. \tag{3}$$

The potential energy is non-dimensionalized by E^*I^*/L^* so that we can write

$$PE_{bending} = \frac{1}{2}\int_0^1 \left(\frac{\partial^2 v(x,t)}{\partial x^2}\right)^2 \mathrm{d}x. \tag{4}$$

The kinetic energy is given by

$$KE^*_{trans} = \frac{1}{2}\int_0^{L^*} \rho^* A^* \left(\frac{\partial v^*(x^*,t^*)}{\partial t^*}\right)^2 \mathrm{d}x^*, \tag{5}$$

where ρ^* is the density of the beam and A^* the cross-sectional area. The cross-sectional area A^* is non-dimensionalized by L^{*2}, and the time t by $1/\omega_1^*$, where ω_1^* is the first natural frequency yet to be determined. The kinetic energy is non-dimensionalized by E^*I^*/L^* so that we can write

$$KE_{trans} = \frac{1}{2}\int_0^1 \rho^* \frac{L^{*6}\omega_1^{*2}}{E^*I^*} A \left(\frac{\partial v(x,t)}{\partial t}\right)^2 \mathrm{d}x \tag{6}$$

By non-dimensionalizing the density ρ^* by $E^*I^*/(L^{*6}\omega_1^{*2})$, we can write

$$KE_{trans} = \frac{1}{2}\int_0^1 \rho A \left(\frac{\partial v(x,t)}{\partial t}\right)^2 \mathrm{d}x. \tag{7}$$

The dimensionless Lagrangian, defined by $KE - PE$, is given by

$$L = \frac{1}{2}\int_0^1 \left[\rho A\left(\frac{\partial v(x,t)}{\partial t}\right)^2 - \left(\frac{\partial^2 v(x,t)}{\partial x^2}\right)^2\right]\mathrm{d}x, \tag{8}$$

The virtual work due to the non-conservative transverse force per unit length $f^*(x^*, t^*)$ is given by

$$\delta W_{nc}^* = \int_0^{L^*} f^*(x^*, t^*)\delta v^*(x^*, t^*)\,\mathrm{d}x^*. \tag{9}$$

Non-dimensionalizing the work by E^*I^*/L^* and the transverse external force f^* by L^{*3}/E^*I^*, the dimensionless non-conservative work is given by

$$\delta W_{nc} = \int_0^1 f(x,t)\delta v(x,t)\,\mathrm{d}x. \tag{10}$$

Using the extended Hamilton's principle, by including the non-conservative forcing, the governing differential equation of motion is given by

$$\rho A\,\frac{\partial^2 v(x,t)}{\partial t^2} + \frac{\partial^4 v(x,t)}{\partial x^4} = f(x,t), \tag{11}$$

with the boundary conditions to be satisfied

$$\frac{\partial^2 v}{\partial x^2}\,\delta\left(\frac{\partial v}{\partial x}\right)\Bigg|_0^1 = 0, \qquad \frac{\partial^3 v}{\partial x^3}\,\delta v\Bigg|_0^1 = 0. \tag{12}$$

Before we go on, let us examine the physical meaning of the boundary conditions above. v is the dimensionless displacement, the first derivative $\partial v/\partial x$ is the dimensionless slope, the second derivative $\partial^2 v/\partial x^2$ is the dimensionless moment, and the third derivative $\partial^3 v/\partial x^3$ is the dimensionless shear. Keep in mind that $\delta v = 0$ means that the variation of the displacement is zero. That is, the displacement is known. It does not necessarily mean that the displacement is zero. Here, we do not consider base excited or end forcing problems. Therefore, only in our case, $\delta v = 0$ or $\delta(\partial v/\partial x) = 0$ means that the displacement or the slope is zero. In order for equation (12) to be satisfied, four combinations of end conditions are possible,

$$\frac{\partial^2 v}{\partial x^2} = 0, \quad v = 0 \text{ for hinged end;} \qquad \frac{\partial v}{\partial x} = 0, \quad v = 0 \text{ for clamped end;}$$

$$\frac{\partial^2 v}{\partial x^2} = 0, \quad \frac{\partial^3 v}{\partial x^3} = 0 \text{ for free end;} \qquad \frac{\partial v}{\partial x} = 0, \quad \frac{\partial^3 v}{\partial x^3} = 0 \text{ for sliding end.} \tag{13}$$

These conditions are shown in Figure 1 where D, S, M, and Q represent displacement, slope, moment and shear respectively.

The equation of motion, boundary conditions, and initial conditions form an initial-boundary-value problem which can be solved using the methods of *separation of variables* and *eigenfunction expansion*. First, we consider a homogeneous problem by setting $f(x,t) = 0$ in order to obtain the natural frequencies and eigenfunctions. By separating $v(x,t)$ into two functions such that $v(x,t) = W(x)T(t)$, the equation of motion (11) can be separated into two ordinary

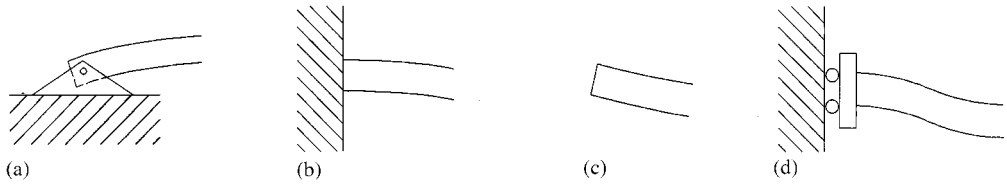

Figure 1. Four types of boundary conditions: (a) hinged, $M(0,t) = 0$, $D(0,t) = 0$; (b) clamped, $D(0,t) = 0$, $S(0,t) = 0$; (c) free, $M(0,t) = 0$, $Q(0,t) = 0$; (d) sliding, $S(0,t) = 0$, $Q(0,t) = 0$.

differential equations,

$$\frac{d^2T(t)}{dt^2} + \omega^2 T(t) = 0, \qquad \frac{d^4W(x)}{dx^4} - a^4 W(x) = 0, \tag{14, 15}$$

where a is related to the angular frequency ω by

$$a^4 = \rho A \omega^2. \tag{16}$$

The quantity a is $1/2\pi$ times the number of cycles in a beam length, and we call a the dimensionless wave number.[†] Equation (16) is called the dispersion relationship. From Equations (14) and (15), $T(t)$ is sinusoidal in time, and $W(x)$ has both sinusoidal and hyperbolic terms:

$$T(t) = d_1 \sin \omega t + d_2 \cos \omega t, \tag{17}$$

$$W(x) = C_1 \sin ax + C_2 \cos ax + C_3 \sinh ax + C_4 \cosh ax, \tag{18}$$

where d_i and C_i are constant coefficients.

Note that the boundary conditions can be expressed in terms of the spatial function $W(x)$ only. For instance, equation (12) can be rewritten as

$$\frac{d^2W}{dx^2}\,\delta\left(\frac{dW}{dx}\right)\Bigg|_0^1 = 0, \qquad \frac{d^3W}{dx^3}\,\delta W\Bigg|_0^1 = 0. \tag{19}$$

from which we can obtain four possible end conditions, as in equation (13), in terms of $W(x)$ only. Now we are ready to apply the boundary conditions to the spatial solution to obtain the corresponding frequency equations and eigenfunctions. This is done is Section 3.2. We proceed next with the Rayleigh beam model.

2.2. THE RAYLEIGH BEAM MODEL

As mentioned in the introduction, the Rayleigh beam adds the rotary inertia effects to the Euler–Bernoulli beam. The variables are non-dimensionalized in the same fashion, and they are tabulated in Appendix A. The kinetic energy due to the

[†] We are defining the wave number as $a^* = 2\pi/\text{wavelength}^*$ so that the dimensionless wave number is given by $a = 2\pi/\text{wavelength}$.

rotation of the cross-section is given by

$$KE_{rot} = \frac{1}{2}\int_0^1 \rho I \left(\frac{\partial^2 v(x,t)}{\partial t \partial x}\right)^2 \mathrm{d}x, \tag{20}$$

where I^* is non-dimensionalized by L^{*4}. Combining equation (20) with equations (4), (7) and (10) to form the Lagrangian and using Hamilton's principle, we obtain the equation of motion given by

$$\rho A \frac{\partial^2 v(x,t)}{\partial t^2} + \frac{\partial^4 v(x,t)}{\partial x^4} - \rho I \frac{\partial^4 v(x,t)}{\partial x^2 \partial t^2} = f(x,t), \tag{21}$$

with the boundary conditions given by

$$\frac{\partial^2 v}{\partial x^2}\,\delta\left(\frac{\partial v}{\partial x}\right)\Bigg|_0^1 = 0, \qquad \left(\frac{\partial^3 v}{\partial x^3} - \rho I \frac{\partial^3 v}{\partial x \partial t^2}\right)\delta v\Bigg|_0^1 = 0, \tag{22}$$

where v is the dimensionless displacement, $\partial v/\partial x$ the dimensionless slope, $\partial^2 v/\partial x^2$ the dimensionless moment and $\partial^3 v/\partial x^3 - \rho I(\partial^3 v/\partial x \partial t^2)$ the dimensionless shear. Four possible end conditions are

$$\frac{\partial^2 v}{\partial x^2} = 0,\ v = 0 \quad \text{for hinged end;} \qquad \frac{\partial v}{\partial x} = 0,\ v = 0 \quad \text{for clamped end;}$$

$$\frac{\partial^2 v}{\partial x^2} = 0, \quad \frac{\partial^3 v}{\partial x^3} - \rho I \frac{\partial^3 v}{\partial x \partial t^2} = 0 \quad \text{for free end;}$$

$$\frac{\partial v}{\partial x} = 0, \quad \frac{\partial^3 v}{\partial x^3} - \rho I \frac{\partial^3 v}{\partial x \partial t^2} = 0 \quad \text{for sliding end.} \tag{23}$$

The expression for shear might seem odd. Its validity can be verified by summing the forces and moments on an incremental beam element, as shown in Figure 2. The sum of the forces on a beam element in the transverse direction is[†]

$$\sum F_y = \rho^* A^* \,\mathrm{d}x^* \frac{\partial^2 v^*}{\partial t^{*2}}$$

$$= -(Q^* + \mathrm{d}Q^*)\cos(\theta + \mathrm{d}\theta) + Q^* \cos\theta + f^*(x^*, t^*)\,\mathrm{d}x^*, \tag{24}$$

where θ can be approximated as $\partial v/\partial x$ or $\partial v^*/\partial x^*$, and $\mathrm{d}Q^*$ and $\mathrm{d}\theta$ represent $(\partial Q^*/\partial x^*)\,\mathrm{d}x^*$ and $(\partial\theta/\partial x^*)\,\mathrm{d}x^*$ respectively. Expanding $\cos(\theta + \mathrm{d}\theta)$ about θ using a Taylor series expansion and using the small angle assumption,[‡] we obtain

$$-\frac{\partial Q^*}{\partial x^*} = \rho^* A^* \frac{\partial^2 v^*}{\partial t^{*2}} - f^*(x^*, t^*). \tag{25}$$

Similarly, taking the sum of the moments about the center of the beam element, we obtain

$$\frac{\partial M^*}{\partial x^*} - Q^* = \rho^* I^* \frac{\partial^3 v^*}{\partial t^{*2} \partial x^*}. \tag{26}$$

[†] Symbols with superscript $*$ are dimensional quantities.

[‡] The small angle assumption means that $\theta^2 \ll 1$.

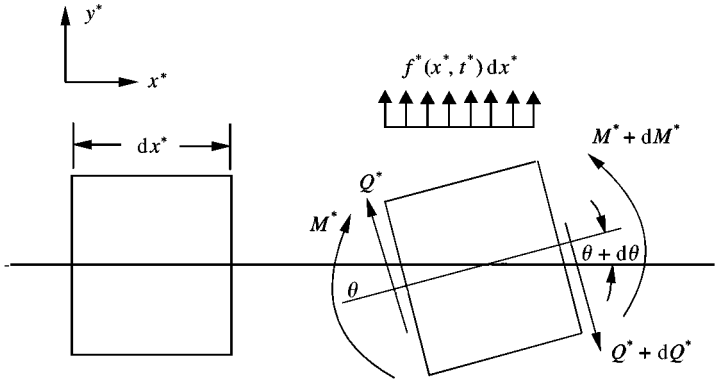

Figure 2. An incremental beam element.

Taking the first derivative of equation (26) with respect to x^*, and subtracting equation (25) from it, we obtain

$$\frac{\partial^2 M^*}{\partial x^{*2}} = \rho^* I^* \frac{\partial^4 v^*}{\partial t^{*2} \partial x^{*2}} - \rho^* A^* \frac{\partial^2 v^*}{\partial t^{*2}} + f^*(x^*, t^*), \tag{27}$$

whose dimensionless form is given by

$$\frac{\partial^2 M}{\partial x^2} = \rho I \frac{\partial^4 v}{\partial t^2 \partial x^2} - \rho A \frac{\partial^2 v}{\partial t^2} + f(x, t). \tag{28}$$

Comparing this with the equation of motion (21), the moment is given by

$$M = \frac{\partial^2 v}{\partial x^2} \quad \text{or} \quad M^* = E^* I^* \frac{\partial^2 v^*}{\partial x^{*2}}. \tag{29}$$

Using equation (29) and (26), the shear is given by

$$Q^* = E^* I^* \frac{\partial^3 v^*}{\partial x^{*3}} - \rho^* I^* \frac{\partial^3 v^*}{\partial t^{*2} \partial x^*}, \tag{30}$$

or

$$Q = \frac{\partial^3 v}{\partial x^3} - \rho I \frac{\partial^3 v}{\partial t^2 \partial x},$$

which verifies our interpretation.

In order to obtain the homogeneous solution, $f(x, t)$ is set equal to zero in equation (21). Separating $v(x, t)$ into spatial and time functions, $v(x, t) = W(x)T(t)$, equation (21) can also be separated into two ordinary differential equations. The time function $T(t)$ obeys the same differential equation as the one for the Euler–Bernoulli model given in equation (14), and the spatial differential equation is given by

$$\frac{\mathrm{d}^4 W(x)}{\mathrm{d}x^4} - \omega^2 \left(\rho A W(x) - \rho I \frac{\mathrm{d}^2 W(x)}{\mathrm{d}x^2} \right) = 0. \tag{31}$$

Again, the time solution $T(t)$ is sinusoidal, and the spatial solution $W(x)$ has both sinusoidal and hyperbolic terms,

$$T(t) = d_1 \sin \omega t + d_2 \cos \omega t, \tag{32}$$

$$W(x) = C_1 \sin ax + C_2 \cos ax + C_3 \sinh bx + C_4 \cosh bx, \tag{33}$$

where the dispersion relations are

$$a = \sqrt{\rho I \omega^2/2 + \sqrt{(\rho I \omega^2/2)^2 + \rho A \omega^2}},$$

$$b = \sqrt{-\rho I \omega^2/2 + \sqrt{(\rho I \omega^2/2)^2 + \rho A \omega^2}}. \tag{34}$$

Note that there are two wave numbers in this case. It will be shown in Section 3.3 that these wave numbers are related only by the slenderness ratio.

The boundary conditions given in equation (22) can be written in terms of $W(x)$ only,

$$\frac{\mathrm{d}^2 W}{\mathrm{d}x^2}\,\delta\left(\frac{\mathrm{d}W}{\mathrm{d}x}\right)\Bigg|_0^1 = 0, \qquad \left(\frac{\mathrm{d}^3 W}{\mathrm{d}x^3} + \rho I \omega^2 \frac{\mathrm{d}W}{\mathrm{d}x}\right)\delta W\Bigg|_0^1 = 0. \tag{35}$$

2.3. THE SHEAR BEAM MODEL

This model adds the effect of shear distortion (but not rotary inertia) to the Euler–Bernoulli model. We introduce new variables α, the angle of rotation of the cross-section due to the bending moment, and β, the angle of distortion due to shear. The total angle of rotation is the sum of α and β and is approximately the first derivative of the deflection,

$$\alpha(x,t) + \beta(x,t) = \partial v(x,t)/\partial x. \tag{36}$$

Therefore, the potential energy due to bending given in equation (4) is slightly modified in this case such that

$$PE_{bending} = \frac{1}{2}\int_0^1 \left(\frac{\partial \alpha(x,t)}{\partial x}\right)^2 \mathrm{d}x. \tag{37}$$

The potential energy due to shear is given by

$$PE^*_{shear} = \frac{1}{2}\int_0^L k' G^* A^* \left(\frac{\partial v^*(x^*,t^*)}{\partial x^*} - \alpha(x^*,t^*)\right)^2 \mathrm{d}x^*. \tag{38}$$

Using the dimensionless length scales and the dimensionless potential energy expressions,

$$PE_{shear} = \frac{1}{2}\int_0^L k' \frac{G^* L^{*4}}{E^* I^*} A \left(\frac{\partial v(x,t)}{\partial x} - \alpha(x,t)\right)^2 \mathrm{d}x. \tag{39}$$

Non-dimensionalizing G^* by $E^* I^*/L^{*4}$, we can write

$$PE_{shear} = \frac{1}{2}\int_0^1 k' GA \left(\frac{\partial v(x,t)}{\partial x} - \alpha(x,t)\right)^2 \mathrm{d}x, \tag{40}$$

TABLE 3

The shear factor

Cross section	k'
Circle	$\frac{6(1+v)}{7+6v}$
Hollow circle with $m = r_{inner}/r_{outer}$	$\frac{6(1+v)(1+m^2)^2}{(7+6v)(1+m^2)^2+(20+12v)m^2}$
Rectangle	$\frac{10(1+v)}{12+11v}$
Thin-walled round tube	$\frac{2(1+v)}{4+3v}$
Thin-walled square tube	$\frac{20(1+v)}{48+39v}$

where k' is the shape factor. Following Cowper's [15] work, some of the values are tabulated in Table 3.

Together with the kinetic energy due to lateral displacement given in equation (7), the Lagrangian is given by

$$L = \frac{1}{2}\int_0^1 \left[\rho A\left(\frac{\partial v(x,t)}{\partial t}\right)^2 - \left(\frac{\partial \alpha(x,t)}{\partial x}\right)^2 - k'GA\left(\frac{\partial v(x,t)}{\partial x} - \alpha(x,t)\right)^2\right]\mathrm{d}x. \quad (41)$$

Unlike in the Euler–Bernoulli and the Rayleigh beam models, there are two dependent variables for the shear beam. The equations of motion, using Hamilton's principle, are given by

$$\rho A\frac{\partial^2 v(x,t)}{\partial t^2} - k'GA\left(\frac{\partial^2 v(x,t)}{\partial x^2} - \frac{\partial \alpha(x,t)}{\partial x}\right) = f(x,t), \quad (42)$$

$$\frac{\partial^2 \alpha(x,t)}{\partial x^2} + k'GA\left(\frac{\partial v(x,t)}{\partial x} - \alpha(x,t)\right) = 0,$$

with the boundary conditions given by

$$\frac{\partial \alpha}{\partial x}\,\delta\alpha\Big|_0^1 = 0, \quad k'GA\left(\frac{\partial v}{\partial x} - \alpha\right)\delta v\Big|_0^1 = 0. \quad (43)$$

v is the dimensionless displacement, α the angle of rotation due to the bending moment, $\partial\alpha/\partial x$ the dimensionless moment, and $k'GA(\partial v/\partial x - \alpha(x,t))$ the dimensionless shear. Four possible boundary conditions are

$$\frac{\partial \alpha}{\partial x} = 0,\ v = 0 \quad \text{for hinged end;}\ \alpha = 0,\ v = 0 \quad \text{for clamped end;} \quad (44)$$

$$\frac{\partial \alpha}{\partial x} = 0,\ k'GA\left(\frac{\partial v}{\partial x} - \alpha\right) = 0 \quad \text{for free end;}\ \alpha = 0,\ \left(\frac{\partial v}{\partial x} - \alpha\right) = 0 \quad \text{for sliding end.}$$

Note that the slope due to the bending moment α is zero (instead of the total slope $\partial v/\partial x$) at the clamped or sliding end.

Now, we try to solve the homogeneous problem without the external forcing function. The two equations of motion (42) can be decoupled to yield

$$\frac{\partial^4 v(x,t)}{\partial x^4} - \frac{\rho}{k'G}\frac{\partial^4 v(x,t)}{\partial x^2 \partial t^2} + \rho A \frac{\partial^2 v(x,t)}{\partial t^2} = 0,$$

$$\frac{\partial^4 \alpha(x,t)}{\partial x^4} - \frac{\rho}{k'G}\frac{\partial^4 \alpha(x,t)}{\partial x^2 \partial t^2} + \rho A \frac{\partial^2 \alpha(x,t)}{\partial t^2} = 0. \tag{45}$$

Note that the forms of the differential equations for v and α are identical.[†] Therefore, we can expect that the forms of $v(x,t)$ and $\alpha(x,t)$ are the same.

The next step is to separate the variables. Here, we first assume that they share the same time solution $T(t)$. In other words, $v(x,t)$ and $\alpha(x,t)$ are synchronized in time,

$$\begin{bmatrix} v(x,t) \\ \alpha(x,t) \end{bmatrix} = T(t) \begin{bmatrix} W(x) \\ \Psi(x) \end{bmatrix}. \tag{46}$$

Now, let us substitute the above expression into the governing differential equation (42) without the term $f(x,t)$ to obtain

$$\rho A W(x) \ddot{T}(t) - k'GA(W''(x) - \Psi'(x))T(t) = 0,$$

$$\Psi''(x)T(t) + k'GA(W'(x) - \Psi(x))T(t) = 0, \tag{47}$$

where the prime and dot notations are used for the derivatives with respect to x and t respectively. The first expression in equation (47) can be separated into two ordinary differential equations given by

$$\ddot{T}(t) + \omega^2 T(t) = 0,$$

$$k'GA(W''(x) - \Psi'(x)) + \omega^2 \rho A W(x) = 0. \tag{48}$$

Again, $T(t)$ is sinusoidal with angular frequency ω as in equation (17). The spatial equations, the second in equation (47) and the second in equation (48), are written using matrix notation as

$$0 = \begin{bmatrix} k'GA & 0 \\ 0 & 1 \end{bmatrix} \begin{bmatrix} W''(x) \\ \Psi''(x) \end{bmatrix} + \begin{bmatrix} 0 & -k'GA \\ k'GA & 0 \end{bmatrix} \begin{bmatrix} W'(x) \\ \Psi'(x) \end{bmatrix} + \begin{bmatrix} \rho A \omega^2 & 0 \\ 0 & -k'GA \end{bmatrix} \begin{bmatrix} W(x) \\ \Psi(x) \end{bmatrix}. \tag{49}$$

These equations can be decoupled to yield

$$W''''(x) + \frac{\rho \omega^2}{k'G} W''(x) - \rho A \omega^2 W(x) = 0,$$

$$\Psi''''(x) + \frac{\rho \omega^2}{k'G} \Psi''(x) - \rho A \omega^2 \Psi(x) = 0. \tag{50}$$

[†] The equations can be decoupled in this way only when the cross-sectional area and the density are uniform.

Note that the differential equations for $W(x)$ and $\Psi(x)$ have the same form, so that we can further assume that the solutions of $W(x)$ and $\Psi(x)$ also have the same form and only differ by a constant as

$$\begin{bmatrix} W(x) \\ \Psi(x) \end{bmatrix} = d\mathbf{u}e^{rx}, \tag{51}$$

where d is the constant coefficient, $\mathbf{u}$ a vector of constant numbers and r the wave number.

When equation (51) is substituted into equation (49), we obtain

$$\begin{bmatrix} k'GAr^2 + \rho A\omega^2 & -k'GAr \\ k'GAr & r^2 - k'GA \end{bmatrix}\mathbf{u} = 0, \tag{52}$$

from which we obtain the eigenvalues r and eigenvectors $\mathbf{u}$. In order to have a non-trivial solution, the determinant of the above matrix has to be zero, that is,

$$r^4 + \frac{\rho\omega^2}{k'G}\, r^2 - \rho A\omega^2 = 0. \tag{53}$$

The eigenvalues are given by

$$r_i = \pm\sqrt{-\frac{\rho\omega^2}{2k'G} \pm \sqrt{\left(\frac{\rho\omega^2}{2k'G}\right)^2 + \rho A\omega^2}} \quad \text{for } i = 1, 2, 3, 4, \tag{54}$$

of which two are real and the other two are imaginary. The corresponding dimensionless eigenvectors $\mathbf{u}_i$ are given by

$$\mathbf{u}_i = \begin{bmatrix} k'GAr_i \\ k'GAr_i^2 + \rho A\omega^2 \end{bmatrix} \quad \text{or} \quad \begin{bmatrix} r_i^2 - k'GA \\ -k'GAr_i \end{bmatrix}. \tag{55}$$

The spatial solution is given by

$$\begin{aligned} \begin{bmatrix} W(x) \\ \Psi(x) \end{bmatrix} &= \sum_{i=1}^{4} d_i\mathbf{u}_i e^{r_i x} \\ &= d_1\mathbf{u}_1 e^{bx} + d_2\mathbf{u}_2 e^{-bx} + d_3\mathbf{u}_3 e^{iax} + d_4\mathbf{u}_4 e^{-iax}, \end{aligned} \tag{56}$$

where

$$a = \sqrt{\frac{\rho\omega^2}{2k'G} + \sqrt{\left(\frac{\rho\omega^2}{2k'G}\right)^2 + \rho A\omega^2}}, \quad b = \sqrt{-\frac{\rho\omega^2}{2k'G} + \sqrt{\left(\frac{\rho\omega^2}{2k'G}\right)^2 + \rho A\omega^2}}. \tag{57}$$

We can write the spatial solution (56) in terms of the sinusoidal and hyperbolic functions with real arguments,

$$\begin{bmatrix} W(x) \\ \Psi(x) \end{bmatrix} = \begin{bmatrix} C_1 \\ D_1 \end{bmatrix}\sin ax + \begin{bmatrix} C_2 \\ D_2 \end{bmatrix}\cos ax + \begin{bmatrix} C_3 \\ D_3 \end{bmatrix}\sinh bx + \begin{bmatrix} C_4 \\ D_4 \end{bmatrix}\cosh bx. \tag{58}$$

It may seem that the spatial solution has eight unknown constant coefficients, C_i and D_i, instead of the four that we started with [d_i in equation (56)]. By expressing the exponential functions $e^{r_i x}$ in equation (56) in terms of sinusoidal and hyperbolic functions, the expressions for the coefficients C_i and D_i are obtained in terms of eigenvectors,

$$\begin{bmatrix} C_1 \\ D_1 \end{bmatrix} = (d_3\mathbf{u}_3 - d_4\mathbf{u}_4)i, \qquad \begin{bmatrix} C_2 \\ D_2 \end{bmatrix} = d_3\mathbf{u}_3 + d_4\mathbf{u}_4,$$

$$\begin{bmatrix} C_3 \\ D_3 \end{bmatrix} = (d_1\mathbf{u}_1 - d_2\mathbf{u}_2), \qquad \begin{bmatrix} C_2 \\ D_2 \end{bmatrix} = d_1\mathbf{u}_1 + d_2\mathbf{u}_2. \tag{59}$$

Keeping in mind that d_3 and d_4 are complex conjugates of each other, we obtain

$$D_1 = -\frac{k'GAa^2 - \rho A\omega^2}{k'GAa} C_2, \qquad D_2 = \frac{k'GAa^2 - \rho A\omega^2}{k'GAa} C_1,$$

$$D_3 = \frac{k'GAb^2 + \rho A\omega^2}{k'GAb} C_4, \qquad D_4 = \frac{k'GAb^2 + \rho A\omega^2}{k'GAb} C_3. \tag{60}$$

Therefore, there are four unknowns. These relations can be obtained more easily by substituting the assumed solution (58) into the spatial differential equations (49).

The boundary conditions in equation (43) are written in terms of spatial solutions as

$$\frac{\mathrm{d}\Psi}{\mathrm{d}x}\,\delta\Psi\Big|_0^1 = 0, \qquad k'GA\left(\frac{\mathrm{d}W}{\mathrm{d}x} - \Psi\right)\delta W\Big|_0^1 = 0. \tag{61}$$

2.4. THE TIMOSHENKO BEAM MODEL

Timoshenko proposed a beam theory which adds the effects of shear distortion and rotary inertia [7, 8] to the Euler–Bernoulli model.† Therefore, the Lagrangian includes the effects of bending moment (37), lateral displacement (7), rotary inertia (20) and shear distortion (40). We assume that there is no rotational kinetic energy associated with shear distortion, but only with the rotation due to bending. Therefore, the kinetic energy term used in the Rayleigh beam (20) is modified to include only the angle of rotation due to bending by replacing $\partial v/\partial x$ with α.

Combining modified equation (20) with equations (7), (37) and (40), the Lagrangian is given by

$$L = \frac{1}{2}\int_0^1 \left[\rho A\left(\frac{\partial v(x,t)}{\partial t}\right)^2 + \rho I\left(\frac{\partial \alpha(x,t)}{\partial t}\right)^2 - \left(\frac{\partial \alpha(x,t)}{\partial x}\right)^2 - k'GA\left(\frac{\partial v(x,t)}{\partial x} - \alpha(x,t)\right)^2\right]\mathrm{d}x. \tag{62}$$

†Equivalently, the Timoshenko model adds rotary inertia to the shear model or adds shear distortion to the Rayleigh model.

The equations of motion are given by

$$\rho A \frac{\partial^2 v(x,t)}{\partial t^2} - k'GA\left(\frac{\partial^2 v(x,t)}{\partial x^2} - \frac{\partial \alpha(x,t)}{\partial x}\right) = f(x,t),$$

$$\rho I \frac{\partial^2 \alpha(x,t)}{\partial t^2} - \frac{\partial^2 \alpha(x,t)}{\partial x^2} - k'GA\left(\frac{\partial v(x,t)}{\partial x} - \alpha(x,t)\right) = 0, \tag{63}$$

and the boundary conditions are given by

$$\frac{\partial \alpha}{\partial x}\,\delta\alpha\Big|_0^1 = 0, \qquad k'GA\left(\frac{\partial v}{\partial x} - \alpha\right)\delta v\Big|_0^1 = 0, \tag{64}$$

which are identical to those of the shear beam.

In order to solve the homogeneous problem, the forcing function is set to zero. The equations of motion (63) can be decoupled into

$$\frac{\partial^4 v}{\partial x^4} - \left(\rho I + \frac{\rho}{k'G}\right)\frac{\partial^4 v}{\partial x^2 \partial t^2} + \rho A \frac{\partial^2 v}{\partial t^2} + \frac{\rho^2 I}{k'G}\frac{\partial^4 v}{\partial t^4} = 0,$$

$$\frac{\partial^4 \alpha}{\partial x^4} - \left(\rho I + \frac{\rho}{k'G}\right)\frac{\partial^4 \alpha}{\partial x^2 \partial t^2} + \rho A \frac{\partial^2 \alpha}{\partial t^2} + \frac{\rho^2 I}{k'G}\frac{\partial^4 \alpha}{\partial t^4} = 0, \tag{65}$$

where it is implied that v and α are functions of x and t. Again, both $v(x,t)$ and $\alpha(x,t)$ obey differential equations of the same form, so that we can make the same argument as we did for the shear beam that $v(x,t)$ and $\alpha(x,t)$ themselves are of the same form.

First, we use the method of separation of variables to separate the equations of motion (63) to obtain the time and the spatial ordinary differential equations. The time equation is the same as the ones for the other models given in equation (14), and the spatial equation is given by

$$0 = \begin{bmatrix} k'GA & 0 \\ 0 & 1 \end{bmatrix}\begin{bmatrix} W''(x) \\ \Psi''(x) \end{bmatrix} + \begin{bmatrix} 0 & -k'GA \\ k'GA & 0 \end{bmatrix}\begin{bmatrix} W'(x) \\ \Psi'(x) \end{bmatrix}$$
$$+ \begin{bmatrix} \rho A\omega^2 & 0 \\ 0 & J\omega^2 - k'GA \end{bmatrix}\begin{bmatrix} W(x) \\ \Psi(x) \end{bmatrix}. \tag{66}$$

Following the procedure used previously from equations (46)–(53), we obtain the characteristic equation

$$r^4 + \left(\rho I + \frac{\rho}{k'G}\right)\omega^2 r^2 - \rho A\omega^2 + \frac{\rho^2 I}{k'G}\,\omega^4 = 0, \tag{67}$$

whose roots are

$$r = \pm\sqrt{-\left(I + \frac{1}{k'G}\right)\frac{\rho\omega^2}{2} \pm \sqrt{\left(I - \frac{1}{k'G}\right)^2 \frac{\rho^2\omega^4}{4} + \rho A\omega^2}}. \tag{68}$$

Of the four roots, the two given by

$$r_{1,2} = \pm \sqrt{-\left(I + \frac{1}{k'G}\right)\frac{\rho\omega^2}{2} - \sqrt{\left(I - \frac{1}{k'G}\right)^2 \frac{\rho^2\omega^4}{4} + \rho A\omega^2}}$$

are always imaginary, and the other two roots given by

$$r_{3,4} = \pm \sqrt{-\left(I + \frac{1}{k'G}\right)\frac{\rho\omega^2}{2} + \sqrt{\left(I - \frac{1}{k'G}\right)^2 \frac{\rho^2\omega^4}{4} + \rho A\omega^2}} \tag{69}$$

are either real or imaginary depending on the frequency ω (for a given material and geometry). They are real when the frequency is less than $\sqrt{k'GA/\rho I}$ and are imaginary when the frequency is greater than $\sqrt{k'GA/\rho I}$. We call this cutoff frequency the critical frequency ω_c. Therefore, we must consider two cases when obtaining spatial solutions: $\omega < \omega_c$ and $\omega > \omega_c$.

When $\omega < \omega_c$, the spatial solution is written in terms of both sinusoidal and hyperbolic terms,

$$\begin{bmatrix} W(x) \\ \Psi(x) \end{bmatrix} = \begin{bmatrix} C_1 \\ D_1 \end{bmatrix} \sin ax + \begin{bmatrix} C_2 \\ D_2 \end{bmatrix} \cos ax + \begin{bmatrix} C_3 \\ D_3 \end{bmatrix} \sinh bx + \begin{bmatrix} C_4 \\ D_4 \end{bmatrix} \cosh bx, \tag{70}$$

where

$$a = \sqrt{\left(I + \frac{1}{k'G}\right)\frac{\rho\omega^2}{2} + \sqrt{\left(I - \frac{1}{k'G}\right)^2 \frac{\rho^2\omega^4}{4} + \rho A\omega^2}},$$

$$b = \sqrt{-\left(I + \frac{1}{k'G}\right)\frac{\rho\omega^2}{2} + \sqrt{\left(I - \frac{1}{k'G}\right)^2 \frac{\rho^2\omega^4}{4} + \rho A\omega^2}}. \tag{71}$$

and C_i and D_i are related by equation (60).

When $\omega > \omega_c$, the spatial solution only has sinusoidal terms,

$$\begin{bmatrix} W(x) \\ \Psi(x) \end{bmatrix} = \begin{bmatrix} \tilde{C}_1 \\ \tilde{D}_1 \end{bmatrix} \sin ax + \begin{bmatrix} \tilde{C}_2 \\ \tilde{D}_2 \end{bmatrix} \cos ax + \begin{bmatrix} \tilde{C}_3 \\ \tilde{D}_3 \end{bmatrix} \sin \tilde{b}x + \begin{bmatrix} \tilde{C}_4 \\ \tilde{D}_4 \end{bmatrix} \cos \tilde{b}x, \tag{72}$$

where

$$a = \sqrt{\left(I + \frac{1}{k'G}\right)\frac{\rho\omega^2}{2} + \sqrt{\left(I - \frac{1}{k'G}\right)^2 \frac{\rho^2\omega^4}{4} + \rho A\omega^2}},$$

$$\tilde{b} = \sqrt{\left(I + \frac{1}{k'G}\right)\frac{\rho\omega^2}{2} - \sqrt{\left(I - \frac{1}{k'G}\right)^2 \frac{\rho^2\omega^4}{4} + \rho A\omega^2}}, \tag{73}$$

and $\tilde{C}_i$ and $\tilde{D}_i$ are related by

$$\tilde{D}_1 = -\frac{k'GAa^2 - \rho A\omega^2}{k'GAa}\tilde{C}_2, \quad \tilde{D}_2 = \frac{k'GAa^2 - \rho A\omega^2}{k'GAa}\tilde{C}_1,$$

$$\tilde{D}_3 = -\frac{k'GA\tilde{b}^2 - \rho A\omega^2}{k'GA\tilde{b}}\tilde{C}_4, \quad \tilde{D}_4 = \frac{k'GA\tilde{b}^2 - \rho A\omega^2}{k'GA\tilde{b}}\tilde{C}_3, \tag{74}$$

Notice that b and $\tilde{b}$ are related by

$$b = \mathrm{i}\tilde{b}. \tag{75}$$

Let us examine the frequency and the wave number where the transition occurs. This critical frequency can be written as

$$\omega_c = \sqrt{\frac{k'GA}{\rho I}} = \frac{1}{k}\sqrt{\frac{k'G}{\rho}}, \tag{76}$$

where k is the dimensionless radius of gyration or the inverse of the slenderness ratio,

$$k = \sqrt{\frac{I^*}{A^*}}\frac{1}{L^*} = \frac{1}{s}. \tag{77}$$

By substituting equation (76) into equations (71) and (73), the critical wave numbers are

$$a_c = \frac{1}{k}\sqrt{(k'GI + 1)}, \qquad b_c = \tilde{b}_c = 0. \tag{78}$$

Writing in terms of dimensional variables

$$a_c = \frac{1}{k}\sqrt{\left(k'\frac{G^*}{E^*} + 1\right)} = \frac{1}{k}\sqrt{\left(\frac{1}{\gamma^2} + 1\right)}, \tag{79}$$

where γ is given by[†]

$$\gamma^2 = \frac{E^*}{k'G^*} = \frac{2(1 + \nu)}{k'}. \tag{81}$$

Recall that k' depends on the Poisson ratio and the shape of the cross-section. Both k' and ν do not vary much so that we can say that the critical wave number essentially depends on the slenderness ratio.

Also, the case when $\omega < \omega_c$ is equivalent to the case when $a < a_c$. This can be verified by taking a derivative of a in the dispersion relationship [equations (71) or (73)] with respect to ω. We will find that the derivative is always positive implying that a is a monotonically increasing function of ω.

3. NATURAL FREQUENCIES AND MODE SHAPES

So far, we have obtained the spatial solutions with four unknowns [equations (18) for the Euler–Bernoulli and Rayleigh models, equations (58) with equation (60) for the shear and the Timoshenko models for $\omega < \omega_c$, and equation (72) with equation (74) for the Timoshenko model for $\omega > \omega_c$], and we have identified the possible boundary conditions that the spatial solutions have to satisfy equation (19)

[†] Here, we use

$$G^* = E^*/2(1 + \nu). \tag{80}$$

for the Euler–Bernoulli, equation (35) for the Rayleigh and equation (61) for the shear and Timoshenko models]. The next step is to apply a set of boundary conditions in order to obtain the four unknown coefficients in the spatial solution. Upon applying the boundary conditions, we obtain four simultaneous equations which can be written as

$$[F]_{4\times 4}\{\mathbf{C}\}_{4\times 1} = \{\mathbf{0}\}_{4\times 1}, \tag{82}$$

where $\{\mathbf{C}\}$ is the vector of coefficients in the spatial solution, and the matrix $[F]$ typically has sinusoidal and hyperbolic functions evaluated at the end points. The determinant of $[F]$ has to be zero to avoid the trivial solution or $\{\mathbf{C}\} = 0$. At this point, the best we can do is to reduce the number of unknowns from four to one. The equation obtained by setting the determinant to zero is the frequency equation, which has an infinite number of roots. For each root, the coefficients C_i of the corresponding spatial solution are unique only to a constant. The roots are in the form of dimensionless wave numbers, which can be translated into natural frequencies using the dispersion relationships. The corresponding spatial solutions are called the eigenfunctions or the mode shapes. The remaining constant in the eigenfunction is usually determined by *normalizing* the modal equation for convenience.[†] In this section, for each model, we obtain the frequency equations, their roots and the mode shapes for four of the ten boundary conditions. Those for the other six cases are obtained using the symmetric and antisymmetric modes.

3.1. SYMMETRIC AND ANTISYMMETRIC MODES

First, let us identify all 10 cases. They are free–free, hinged–hinged, clamped–clamped, clamped–free, sliding–sliding, free–hinged, free–sliding, clamped–hinged, clamped–sliding and hinged–sliding supports. Using the symmetric and antisymmetric modes, we try to minimize the cases to be considered.

Excluding the rigid-body mode, the free–sliding is the symmetric mode[‡] and the free–hinged is the antisymmetric mode of the free–free case as shown in Figure 3.

Similarly, the clamped–sliding is the symmetric mode and the clamped–hinged is the antisymmetric mode of the clamped–clamped case. The hinged–sliding is the symmetric mode of the hinged–hinged case and the antisymmetric mode of the sliding–sliding case.

Once we obtain the dimensionless wave numbers of the free–free, hinged–hinged, clamped–clamped, and clamped–free cases, we can find the dimensionless wave numbers of the remaining cases using the definition of the dimensionless wave number. The dimensionless wave number is $1/2\pi$ times the number of cycles contained in the beam length. As shown in Figure 3 for the free–free beam, the

[†] see sections 5.1 and 5.2 for normalization process.

[‡] The symmetric mode of the free–free beam requires that the total slope of the beam $v'(x,t)$ in the middle of the beam is zero. On the other hand, for the shear and Timoshenko models, the free–sliding beam requires that the angle of rotation due to bending α is zero at the sliding end. It seems that the symmetric mode of the free–free beam cannot represent the free–sliding beam. However, if we look more closely, the other condition for the sliding end is that $\beta = 0$ which leads to $v' = 0$. Therefore, the free–sliding beam can be replaced by the symmetric mode of the free–free beam.

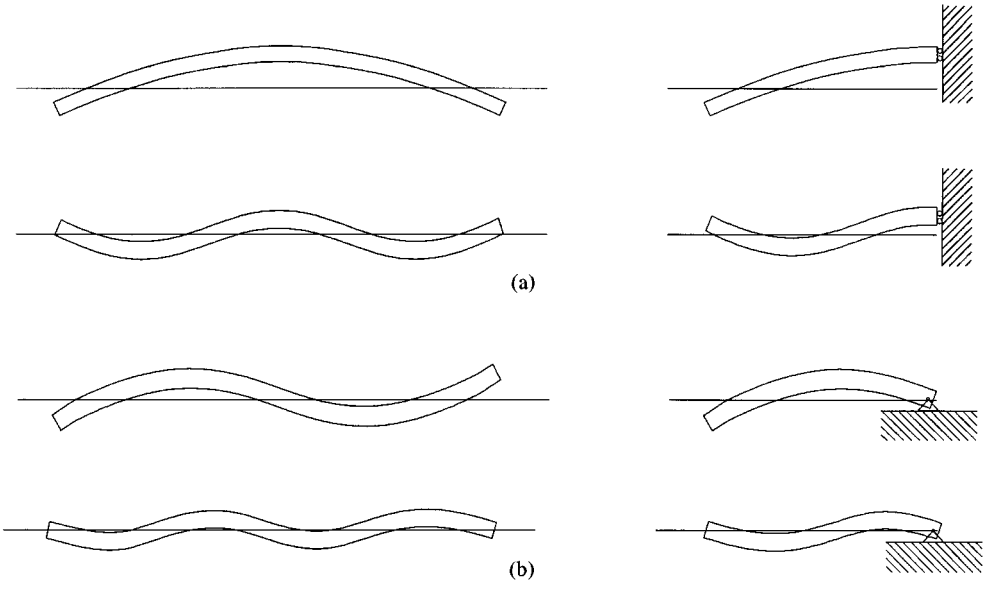

Figure 3. The (a) symmetric and (b) antisymmetric modes of the free–free beam.

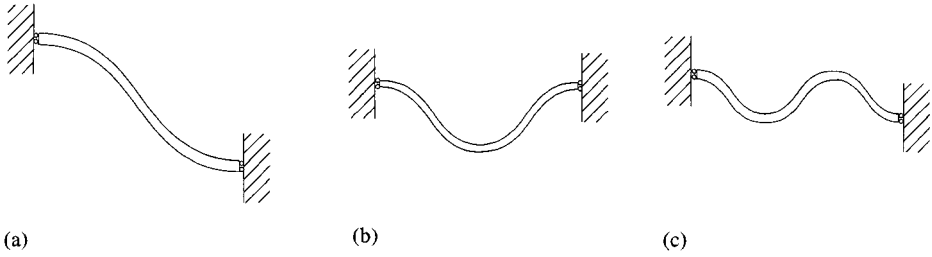

Figure 4. The first three modes of the sliding–sliding beam: (a) first, (b) second, (c) third.

symmetric (free–sliding) and the antisymmetric (free–hinged) cases contain half of the cycles contained in the free–free case. Therefore, the dimensionless wave numbers are also half of that of the free–free case. The dimensionless wave numbers are related as shown in Table 4. Keep in mind that the rigid-body mode ($a_1 = 0$) is omitted for the free–sliding, free–hinged, free–free, sliding–sliding cases. Note that the first mode of the free–free and the clamped–clamped cases are symmetric whereas the first mode of sliding–sliding case is antisymmetric as shown in Figure 4.

From the last four relations in Table 4, we can further deduce that the sliding–sliding support case is the same as the hinged–hinged case. Therefore, there are only four cases to be considered: free–free, hinged–hinged, clamped–clamped, clamped–free. Similarly, the mode shapes of these four cases can be used to generate the mode shapes of the other six cases. For instance, the first and third mode shapes (symmetric modes) of the free–free case generate the first and second mode shapes of the free–sliding case (excluding the rigid-body mode), and the second and fourth mode shapes (antisymmetric modes) generate the first and

TABLE 4

The relationship between normalized wave numbers of various boundary conditions for $n = 1, 2, 3, \ldots$

1. $a_n^{free-sliding} = \frac{1}{2}a_{2n-1}^{free-free}$	5. $a_n^{hinged-sliding} = \frac{1}{2}a_{2n-1}^{hinged-hinged}$
2. $a_n^{free-hinged} = \frac{1}{2}a_{2n}^{free-free}$	6. $a_n^{hinged-hinged} = \frac{1}{2}a_{2n}^{hinged-hinged}$
3. $a_n^{clamped-sliding} = \frac{1}{2}a_{2n-1}^{clamped-clamped}$	7. $a_n^{sliding-sliding} = \frac{1}{2}a_{2n}^{sliding-sliding}$
4. $a_n^{clamped-hinged} = \frac{1}{2}a_{2n}^{clamped-clamped}$	8. $a_n^{sliding-hinged} = \frac{1}{2}a_{2n-1}^{sliding-sliding}$

second mode shapes of the free–hinged case as shown in Figure 3. Similarly, mode shapes of the sliding–sliding case can be generated by hinged–hinged case.

It is important to note that it is implied in Figure 3 that the cross-sectional areas of the beams are the same, and the lengths of the free–sliding or free–hinged beams are half of the free–free beam. In fact, this does not always have to be the case. As long as the slenderness ratio of the free–free beam is twice that of the free–sliding or free–hinged beam, this analysis works. Therefore, more precisely, we can say that the dimensionless wave numbers of the free–free beam with the slenderness ratio of s is twice the dimensionless wave numbers of the free–sliding or free–hinged case with the slenderness ratio of $s/2$.

3.2. THE EULER-BERNOULLI BEAM MODEL

The spatial solution $W(x)$ is given in equation (18), and the expressions for the boundary conditions are given in equation (13). Here the dimensionless wave numbers are obtained by applying the four sets of boundary conditions to the spatial solution.

One special characteristic of this model is that the frequency equations for the free–free and clamped–clamped cases are the same. This is the case only for this model. The frequency equations for four cases and the first five dimensionless wave numbers are tabulated in Table 5. The wave numbers for the remaining cases, using Table 4, are tabulated in Table 6. Note that we were able to obtain the numerical values for the dimensionless wave numbers. It will be shown that for other models, it is not possible to do so.

The actual frequency of vibration can be found using the dispersion relationship in equation (16). That is,

$$\omega^* = \sqrt{\frac{E^*I^*}{\rho^*A^*L^{*4}}}\, a^2. \tag{83}$$

Using the dispersion relationship, we can also write

$$\omega_n^* L^* \sqrt{\rho^*/E^*} = \frac{a_n^2}{s}, \tag{84}$$

so that we can plot $\omega_n^* L^* \sqrt{\rho^*/E^*}$ as a function of $1/s$. This will be useful when we compare the natural frequencies predicted by other models.

TABLE 5

The frequency equations and the first five wave numbers of Euler–Bernoulli model

	The frequency equation	a_1	a_2	a_3	a_4	a_5
c-c and f-f	$\cos a \cosh a - 1 = 0$	4·730	7·853	10·996	14·137	17·279
h-h or s-s	$\sin a \sinh a = 0$	π	2π	3π	4π	5π
c-f	$\cos a \cosh a + 1 = 0$	1·875	4·694	7·855	10·996	14·137

TABLE 6

The first five wave numbers obtained using the symmetric and antisymmetric modes

	a_1	a_2	a_3	a_4	a_5
c-s and f-s	2·365	5·498	8·639	11·781	14·923
c-h and f-h	3·927	7·069	10·210	13·352	16·493
h-s	$0{\cdot}5\pi$	$1{\cdot}5\pi$	$2{\cdot}5\pi$	$3{\cdot}5\pi$	$4{\cdot}5\pi$

3.3. THE RAYLEIGH BEAM MODEL

The expressions for the boundary conditions are given in equation (23). Unlike in the Euler–Bernoulli beam case, there are two wave numbers in the Rayleigh beam, a and b.† The frequency equation will have both a and b. In order to find the solution to the frequency equations, one of the wave numbers has to be expressed in terms of the other so that the frequency equation is a function of one wave number only, let us say a. Following is the procedure used to express b in terms of a.

The dispersion relations given in equation (34) can be written as

$$a^2 = B_1 + \sqrt{B_1^2 + B_2}, \qquad b^2 = -B_1 + \sqrt{B_1^2 + B_2}, \tag{85}$$

where B_1 and B_2, in this case, are

$$B_1 = \frac{\rho I \omega^2}{2}, \qquad B_2 = \rho A \omega^2. \tag{86}$$

Solving for B_1 and B_2 in equation (85) we obtain

$$B_1 = (a^2 - b^2)/2, \qquad B_2 = a^2 b^2 \tag{87}$$

Note that equations (87) are still the dispersion relations. Now, let us examine the ratio of B_1 to B_2. From equations (87) and (86),

$$\frac{B_1}{B_2} = \frac{1}{2}\left(\frac{1}{b^2} - \frac{1}{a^2}\right) = \frac{I}{2A}, \tag{88}$$

† Note that the wave number of a hyperbolic function, b, does not have a physical meaning while the wave number of a sinusoidal function, a, does. Nonetheless, we call b the wave number of the hyperbolic function.

TABLE 7

The frequency equations of the Rayleigh model

f-f	$(b^6 - a^6)\sin a \sinh b + 2a^3b^3 \cos a \cosh b - 2a^3b^3 = 0$
c-c	$(b^2 - a^2)\sin a \sinh b - 2ab \cos a \cosh b + 2ab = 0$
h-h or s-s	$\sin a \sinh b = 0$
c-f	$(b^2 - a^2)ab \sin a \sinh b + (b^4 + a^4)\cos a \cosh b + 2a^2b^2 = 0$

where the ratio of I to A is k^2 from equation (77). Now, we can write

$$\frac{1}{b^2} - \frac{1}{a^2} = k^2 = \frac{1}{s^2}. \tag{89}$$

Therefore, the wave numbers of the Rayleigh beam are related by the slenderness ratio. This contrasts with the case of the Euler–Bernoulli beam where the dimensionless wave numbers are independent of the geometry of the beam but dependent solely on the boundary conditions. Expressing b in terms of a and k (or s),

$$b = a\sqrt{\frac{1}{a^2k^2 + 1}} = as\sqrt{\frac{1}{a^2 + s^2}}. \tag{90}$$

Let us consider the case when $k = 0$. Then, a equals b by equation (89) or (90), and B_1 is zero by equation (87). Comparing equation (85) with equation (16), we also find that the wave numbers a and b are equal to the wave number of the Euler–Bernoulli beam. For a slender beam where s is large (k is small), the two wave numbers approach each other so that the result resembles that of the Euler–Bernoulli beam.†

The frequency equations for four cases are given in Table 7. Notice that the frequency equations contain both a and b as predicted earlier. Further, notice that when b is expressed in terms of a using equation (90), the geometrical property, slenderness ratio, enters the frequency equations. Therefore, the roots of the frequency equations depend on the slenderness of the beam and are no longer independent of the geometry of the beam. The significance of the previous statement is that it implies that the mode shapes also vary with the slenderness ratio.

As mentioned earlier, as s approaches infinity, the frequency equation becomes identical to that of the Euler–Bernoulli beam. The best way to represent the solution of the frequency equation is to plot wave numbers as a continuous function of s or k. Here, we will use k for a reason which will become apparent shortly. The frequency equations in Table 7 are transcendental equations that have to be solved numerically. In order to obtain a smooth function, $a(k)$, we use the following analysis. Let one of the frequency equations be $F(a, b)$. From equation

† In general, the slenderness ratio of 100 is sufficient so that there is little difference among all four models (Euler–Bernoulli, Rayleigh, shear and Timoshenko).

(90), b is a function of a and k, $b(a, k)$. dF and db are given by

$$\mathrm{d}F = \frac{\partial F}{\partial a}\,\mathrm{d}a + \frac{\partial F}{\partial b}\,\mathrm{d}b, \qquad \mathrm{d}b = \frac{\partial b}{\partial a}\,\mathrm{d}a + \frac{\partial b}{\partial k}\,\mathrm{d}k. \tag{91}$$

Combining two expressions, dF is given by

$$\mathrm{d}F = \frac{\partial F}{\partial a}\,\mathrm{d}a + \frac{\partial F}{\partial b}\left(\frac{\partial b}{\partial a}\,\mathrm{d}a + \frac{\partial b}{\partial k}\,\mathrm{d}k\right) = 0, \tag{92}$$

where dF is zero because F is zero. Solving for da/dk, we obtain

$$\frac{\mathrm{d}a}{\mathrm{d}k} = \frac{-(\partial F/\partial b)(\partial b/\partial k)}{(\partial F/\partial a) + (\partial F/\partial b)(\partial b/\partial a)}, \tag{93}$$

where the right-hand side is a function of a, b and k. After b is expressed in terms of a and k by equation (90), the right-hand side is a function of a and k only. Now, this is a first order ordinary differential equation which can be solved once we know the initial value $a(k = 0)$. The initial value is identical to the wave numbers of the Euler–Bernoulli model given in Tables 5 and 6. Note that depending on which wave number we use as an initial value, $a_1, a_2, \ldots$, we can track that particular wave number as the slenderness ratio varies. The initial value problem is solved using MATLAB, and the results are shown in Figures 5–8. The four solid lines in each figure are the wave numbers obtained using the Euler–Bernoulli theory. They are not affected by the slenderness ratio. The two lines (dotted and dot-dashed) that emerge from nth solid line near $1/s = 0$ are the nth waves numbers, a_n and b_n, of the

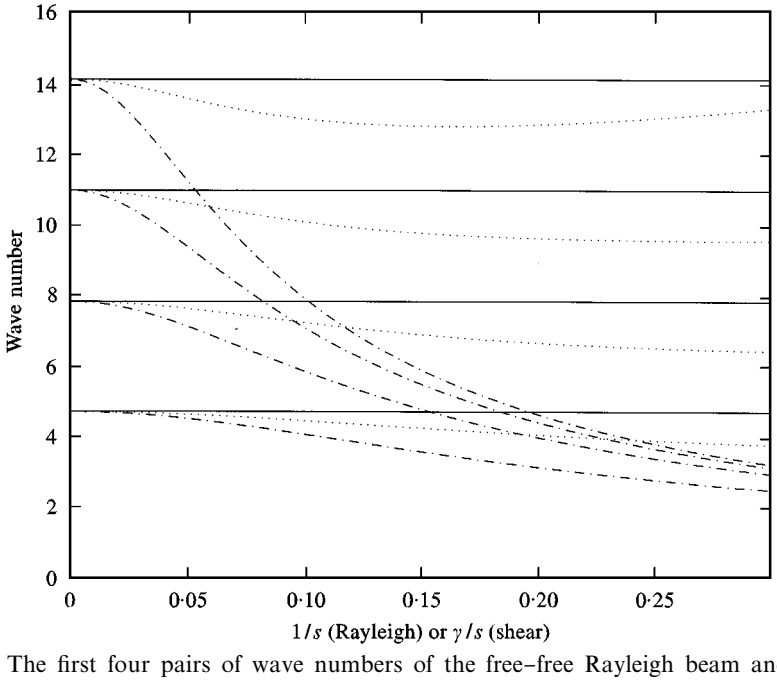

Figure 5. The first four pairs of wave numbers of the free–free Rayleigh beam and clamped–clamped shear beam: —, Euler–Bernoulli; ···, a; –·–·–, b.

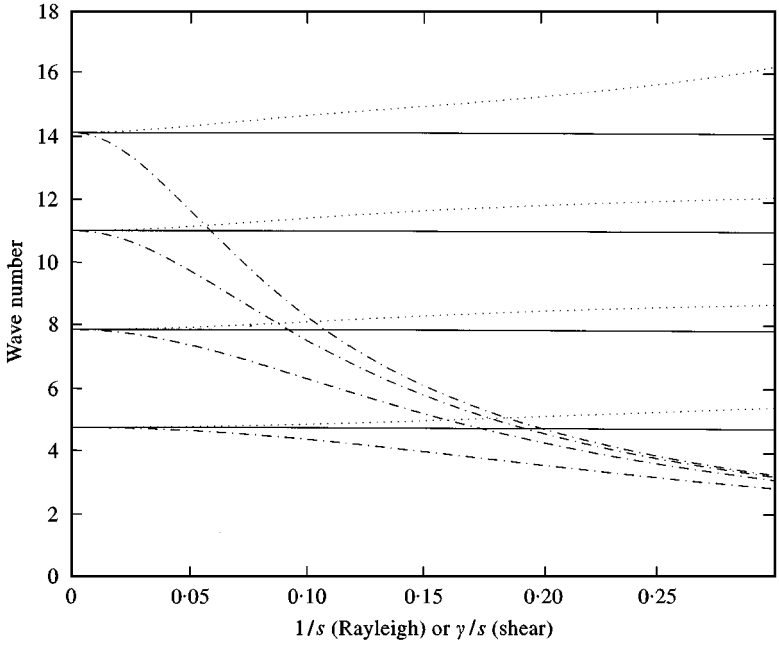

Figure 6. The first four pairs of wave numbers of the clamped–clamped Rayleigh beam and free–free shear beam: —, Euler–Bernoulli; ···, a; –·–·–, b.

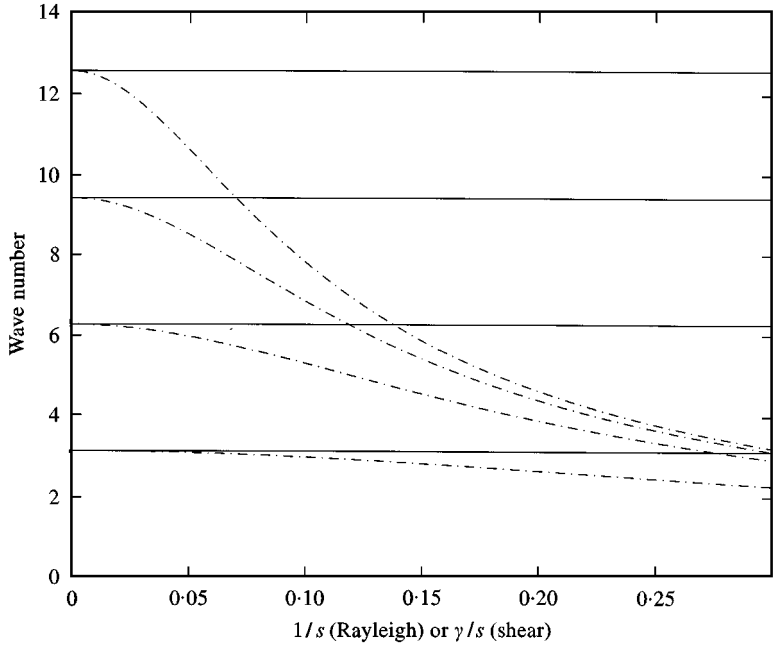

Figure 7. The first four pairs of wave numbers of the hinged–hinged (or sliding–sliding) Rayleigh and shear beam: —, Euler–Bernoulli or a; –·–·–, b.

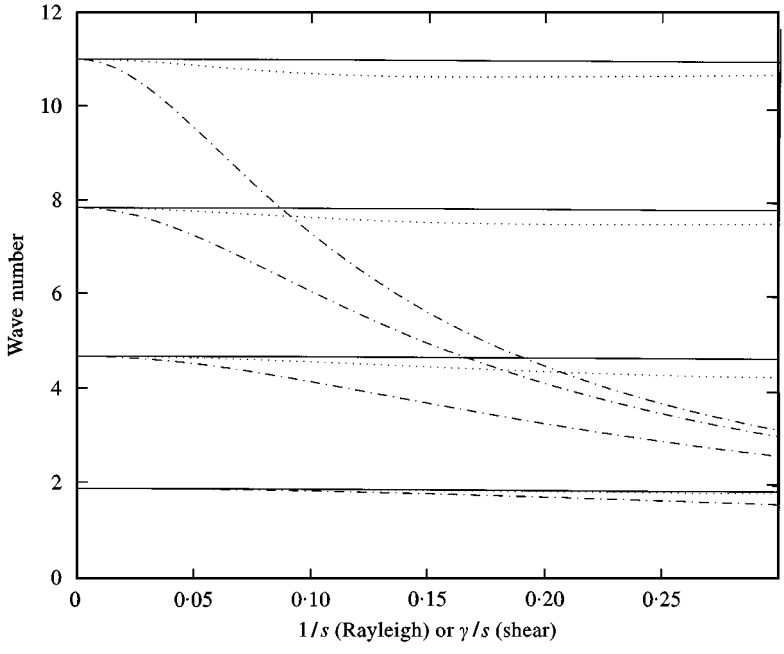

Figure 8. The first four pairs of wave numbers of the clamped–free Rayleigh and shear beam: —, Euler–Bernoulli; ⋯, a; –·–·–, b.

Rayleigh model. Using these plots, we obtain up to four sets of wave numbers for each case.

Having such plots, we can instantly obtain the dimensionless wave numbers once we know the slenderness ratio. These dimensionless wave numbers together with the complete properties of the beam lead to the natural frequencies using the dispersion relations. The natural frequency, solved in terms of the wave numbers and the property of the beam using the dispersion relations (86) and (87), is given by

$$\omega^2 = \frac{a^2 - b^2}{\rho I} \quad \text{or} \quad \omega^2 = \frac{a^2 b^2}{\rho A}, \tag{94}$$

which is equivalent to

$$\omega^{*2} = (a^2 - b^2)\frac{E^*}{\rho^* L^{*2}} \quad \text{or} \quad \omega^{*2} = \frac{a^2 b^2}{s^2}\frac{E^*}{\rho^* L^{*2}}. \tag{95}$$

Since we know a and b as discrete functions of $1/s$ from Figures 5–8, we can plot $\omega^* L^* \sqrt{\rho^*/E^*}$ as a function of $1/s$ using the first relation in equation (95),

$$\omega^* L^* \sqrt{\rho^*/E^*} = \sqrt{a^2 - b^2}. \tag{96}$$

The plots of $\omega^* L^* \sqrt{\rho^*/E^*}$ as a function of $1/s$ are shown in Figures 9–12. The benefit of having such plots is that once we know s, L^*, ρ^*, and E^*, ω^* can be obtained instantly. For example, the first four pairs of wave numbers of the clamped–free Rayleigh beam when $s = 9{\cdot}1192$ (or $1/s = 0{\cdot}11$) can be obtained from Figure 8 and the natural frequencies, where $L^* = 1$ m, $\rho^* = 7830\ \text{kg/m}^3$, and

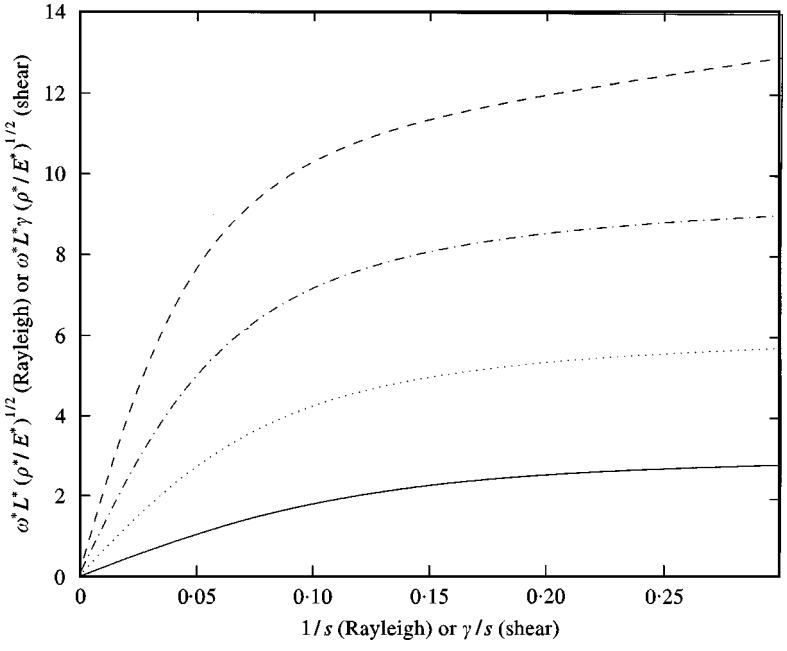

Figure 9. The frequency curves for the free–free Rayleigh and clamped–clamped shear beam; —, ω_1^* …; ⋯, ω_2^* …; –·–·–, ω_3^* …; – – –, ω_4^* ….

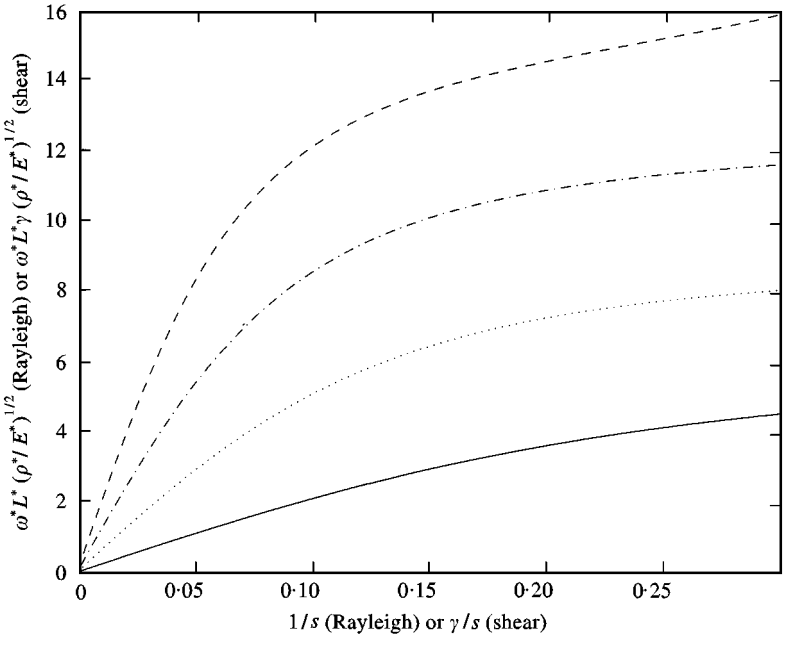

Figure 10. The frequency curves for the clamped–clamped Rayleigh and free–free shear beam; —, ω_1^* …; ⋯, ω_2^* …; –·–·–, ω_3^* …; – – –, ω_4^* ….

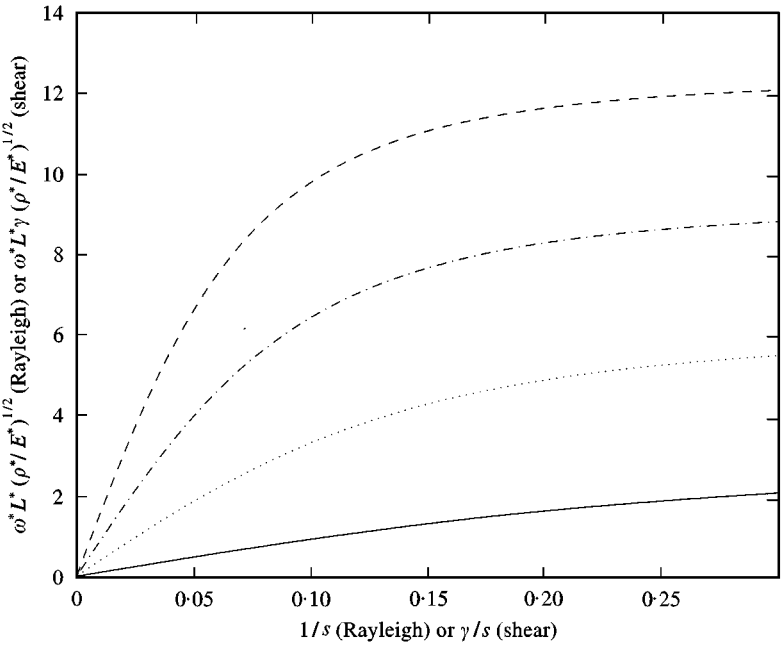

Figure 11. The frequency curves for the hinged–hinged (or sliding–sliding) Rayleigh and shear beam; —, ω_1^* …; ⋯, ω_2^* …; –·–·–, ω_3^* …; – – –, ω_4^* ….

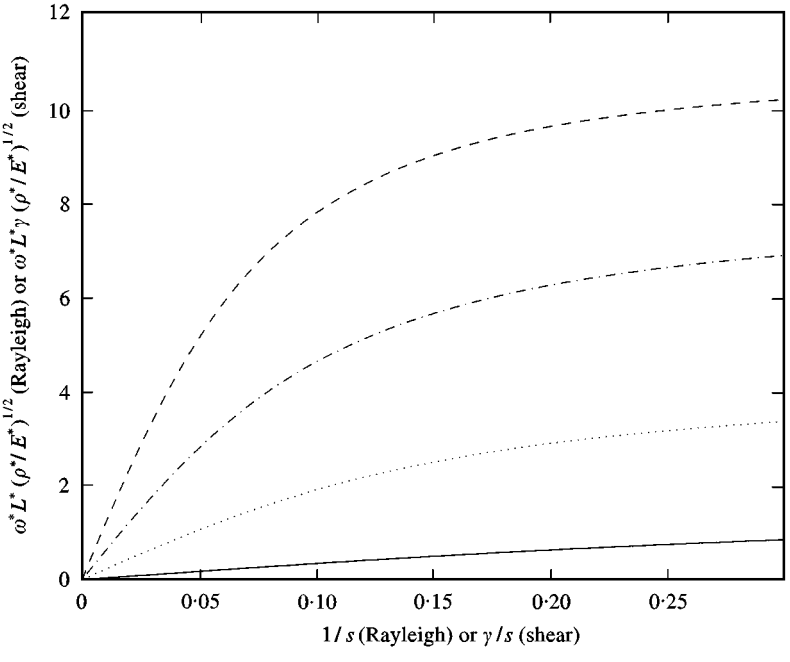

Figure 12. The frequency curves for the clamped–free Rayleigh and shear beam; —, ω_1^* …; ⋯, ω_2^* …; –·–·–, ω_3^* …; – – –, ω_4^* ….

$E^* = 200$ GPa, can be obtained from Figure 12. The exact numbers are

$$(a_1, b_1) = (1{\cdot}869, 1{\cdot}831),\ \omega_1 = 1; \qquad (a_2, b_2) = (4{\cdot}571, 4{\cdot}086), \quad \omega_2 = 5{\cdot}459;$$

$$(a_3, b_3) = (7{\cdot}629, 5{\cdot}851),\ \omega_3 = 13{\cdot}046; \qquad (a_4, b_4) = (10{\cdot}686, 6{\cdot}937), \quad \omega_4 = 21{\cdot}664. \tag{97}$$

Note that the natural frequencies are non-dimensionalized by the first natural frequency given by $\omega_1^* = 1896$ rad/s. These numbers will be used in the example problem at the end of this paper.

One comment is made here regarding the wave numbers and the frequency charts for the other six sets of boundary conditions. It was mentioned earlier that the dimensionless wave numbers of the free–free beam with the slenderness ratio of s are twice the dimensionless wave numbers of the free–sliding or free–hinged case with the slenderness ratio of $s/2$, where the same analogy is applied to the other cases: the clamped–clamped and hinged–hinged beams. For example, the wave numbers of the free–sliding beam are obtained from the wave numbers of the odd modes of free–free beams $(a_1, b_1), (a_3, b_3), \ldots$ by replacing the abscissa label $1/s$ with $1/(2s)$ and ordinate label wave numbers with $2 \times$ (wave numbers) in Figure 5. In this way, a point that corresponds to the inverse slenderness ratio of $1/s_0$ and wave numbers of a_0 and b_0 in Figure 5, would correspond to the inverse slenderness ratio of $2/s_0$ and the wave numbers of $a_0/2$ and $b_0/2$ in the new plot. The frequency charts can be modified in the same way so that the abscissa label $1/s$ is replaced by $1/(2s)$ and the wave numbers in ordinate label, $\sqrt{a^2 - b^2}$, are replaced by $2 \times$(wave number) so that the new ordinate label is $2\sqrt{a^2 - b^2}$ or $2\omega^* L^* \sqrt{\rho^*/E^*}$. The wave numbers and the frequency charts of the shear and Timoshenko models are obtained in the same way.

3.4. THE SHEAR BEAM MODEL

The same analysis as for the Rayleigh beam is applied here. Again, the dispersion relationship given in equation (57) is written in the form of equation (85) where B_1 and B_2 are given by

$$B_1 = \frac{\rho\omega^2}{2k'G}, \quad B_2 = \rho A\omega^2 \tag{98}$$

and

$$B_1 = (a^2 - b^2)/2, \qquad B_2 = a^2 b^2. \tag{99}$$

The latter relations are identical to those of the Rayleigh beam (87). Using equation (99), the ratio of B_1 to B_2 is reduced to

$$\frac{B_1}{B_2} = \frac{1}{2}\left(\frac{1}{b^2} - \frac{1}{a^2}\right), \tag{100}$$

TABLE 8

The frequency equations of the shear model

f-f	$(b^2 - a^2)\sin a \sinh b - 2ab \cos a \cosh b + 2ab = 0$
c-c	$(b^6 - a^6)\sin a \sinh b + 2a^3b^3 \cos a \cosh b - 2a^3b^3 = 0$
h-h or s-s	$\sin a \sinh b = 0$
c-f	$(b^2 - a^2)ab \sin a \sinh b + (b^4 + a^4)\cos a \cosh b + 2a^2b^2 = 0$

and using equation (98) the ratio is reduced to

$$\frac{B_1}{B_2} = \frac{1}{2k'GA} = \frac{E^*I^*L^{*2}}{2k'G^*L^{*4}A^*} = \frac{(1+\nu)}{k'}\frac{1}{s^2} = \frac{1}{2}\left(\frac{\gamma}{s}\right)^2, \tag{101}$$

where γ is given in equation (81) and G^* is related to E^* by equation (80). Therefore, we can write

$$\left(\frac{1}{b^2} - \frac{1}{a^2}\right) = \left(\frac{\gamma}{s}\right)^2 = (\gamma k)^2. \tag{102}$$

Solving for b, we obtain

$$b = a\sqrt{\frac{1}{\gamma^2k^2a^2 + 1}} = \frac{as}{\gamma}\sqrt{\frac{1}{a^2 + s^2/\gamma^2}}. \tag{103}$$

Looking again at equation (60), we find that the coefficients in the spatial solutions are related by

$$D_1 = -\frac{b^2}{a}C_2, \qquad D_2 = \frac{b^2}{a}C_1, \qquad D_3 = \frac{a^2}{b}C_4, \qquad D_4 = \frac{a^2}{b}C_3, \tag{104}$$

so that we can write the spatial solution in terms of the wave numbers only.

The frequency equations for the shear beam are given in Table 8. Note that the frequency equation for the free–free shear beam is identical to the clamped–clamped Rayleigh beam. Also, the frequency equation for the clamped–clamped shear beam is identical to that of the free–free Rayleigh beam. The frequency equations for the other two cases are the same as the ones for the Rayleigh beam. Also note that the relationship between wave numbers (102) is similar to that of the Rayleigh beam (89). In fact, $1/s$ is modified by the factor γ. We can use the plots for the Rayleigh beam here by just replacing the label for the abscissa $1/s$ with γ/s and switching the free–free case with the clamped–clamped case. The clamped–clamped case is shown in Figure 5, free–free in Figure 6, hinged–hinged (or sliding–sliding) in Figure 7, and clamped–free in Figure 8.

From equations (98) and (99), the natural frequency is given by

$$\sqrt{\frac{\rho^*L^{*2}}{E^*}}\sqrt{\frac{2(1+\nu)}{k'}}\,\omega^* = \sqrt{a^2 - b^2}, \tag{105}$$

where $\sqrt{2(1+\nu)/k'}$ is denoted as γ throughout this paper as shown in equation (81). Notice the similarity between equations (96) and (105). Therefore, we can use

the plots used in the Rayleigh beam (Figures 9–12) by simply replacing the ordinate with $\omega^* L^* \gamma \sqrt{\rho^*/E^*}$. The notation $\omega_n^* \ldots$ in the captions are representative of $\omega_n^* L^* \sqrt{\rho^*/E^*}$ for the Rayleigh and $\omega_n^* L^* \gamma \sqrt{\rho^*/E^*}$ for the shear model.

Again, these plots are convenient for easily obtaining the natural frequencies for a given s and γ. From Figures 8 and 12, for $1/s = 0{\cdot}11$, $L^* = 1$ m, $\gamma = 2{\cdot}205$, $\rho^* = 7830\ \text{kg/m}^3$, and $E^* = 200$ GPa, the pairs of wave numbers and the natural frequencies are

$$\begin{aligned} &(a_1, b_1) = (1{\cdot}846, 1{\cdot}686),\ \omega_1 = 1; \qquad (a_2, b_2) = (4{\cdot}352, 2{\cdot}998), \quad \omega_2 = 4{\cdot}1923; \\ &(a_3, b_3) = (7{\cdot}539, 3{\cdot}626),\ \omega_3 = 8{\cdot}7823; \qquad (a_4, b_4) = (10{\cdot}686, 3{\cdot}857), \quad \omega_4 = 13{\cdot}241; \end{aligned} \tag{106}$$

where the natural frequencies are non-dimensionalized by the first natural frequency $\omega_1^* = 1725$ rad/s.

3.5. THE TIMOSHENKO BEAM MODEL

Here, we follow the same procedure used for the Rayleigh and the shear beams by letting

$$B_1 = \frac{\rho I \omega^2}{2}, \qquad B_2 = \frac{\rho \omega^2}{2k'G} = B_1 \gamma^2, \qquad B_3 = \rho A \omega^2, \tag{107}$$

so that the dispersion relations in equations (71) and (73) can be written as

$$\begin{aligned} a &= \sqrt{(B_1 + B_2) + \sqrt{(B_1 - B_2)^2 + B_3}}, \\ b &= \sqrt{-(B_1 + B_2) + \sqrt{(B_1 - B_2)^2 + B_3}} = i\tilde{b}. \end{aligned} \tag{108}$$

Solving for B_1, B_2 and B_3, we obtain

$$\begin{aligned} B_1 &= \frac{a^2 - b^2}{2(1 + \gamma^2)}, \qquad B_2 = \frac{\gamma^2 (a^2 - b^2)}{2(1 + \gamma^2)}, \\ B_3 &= \frac{1}{4}\left\{(a^2 + b^2)^2 - \frac{(1 - \gamma^2)^2}{(1 + \gamma^2)^2}\,(a^2 - b^2)^2\right\}, \end{aligned} \tag{109}$$

where γ is a constant given in equation (81). Note that B_1, B_2, and B_3 can be obtained in terms of a and $\tilde{b}$ by replacing b^2 with $\tilde{b}^2$ in equation (109). By equating the ratio of B_3 to B_1 using equations (107) and (109), we obtain the relationship between the wave numbers given by

$$\frac{(\gamma^2 b^2 + a^2)(a^2 \gamma^2 + b^2)}{(a^2 - b^2)(1 + \gamma^2)} = s^2. \tag{110}$$

Again, the relationship between a and $\tilde{b}$ can be obtained by replacing b with $i\tilde{b}$ in equation (110) as

$$\frac{(-\gamma^2 \tilde{b}^2 + a^2)(\gamma^2 a^2 - \tilde{b}^2)}{(a^2 + \tilde{b}^2)(1 + \gamma^2)} = s^2. \tag{111}$$

Note that the wave numbers are related by s and γ.

Using equations (107) and (109), we can write equation (60) as

$$D_1 = -\frac{a^2 + \gamma^2 b^2}{(1+\gamma^2)a} C_2, \qquad D_2 = \frac{a^2 + \gamma^2 b^2}{(1+\gamma^2)a} C_1,$$
$$D_3 = \frac{b^2 + \gamma^2 a^2}{(1+\gamma^2)b} C_4, \qquad D_4 = \frac{b^2 + \gamma^2 a^2}{(1+\gamma^2)b} C_3, \tag{112}$$

so that the spatial solution for $\omega < \omega_c$ can be written in terms of wave numbers only. Using equations (107) and (109) with b replaced by $\mathrm{i}\tilde{b}$, the coefficients $\tilde{C}_i$ and $\tilde{D}_i$ in equation (74) are then related by

$$\tilde{D}_1 = -\frac{a^2 - \gamma^2 \tilde{b}^2}{(1+\gamma^2)a} \tilde{C}_2, \qquad \tilde{D}_2 = \frac{a^2 - \gamma^2 \tilde{b}^2}{(1+\gamma^2)a} \tilde{C}_1,$$
$$\tilde{D}_3 = -\frac{\tilde{b}^2 - \gamma^2 a^2}{(1+\gamma^2)\tilde{b}} \tilde{C}_4, \qquad \tilde{D}_4 = \frac{\tilde{b}^2 - \gamma^2 a^2}{(1+\gamma^2)\tilde{b}} \tilde{C}_3, \tag{113}$$

which we can use to express the spatial solution for $\omega > \omega_c$ in terms of the wave numbers only.

Note that we only need to obtain one frequency equation for each boundary condition. Once the frequency equation for the case $a < a_c$ is obtained, the other frequency equation for $a > a_c$ can be obtained by replacing b with $\mathrm{i}\tilde{b}$. The frequency equations for the case $a < a_c$ are tabulated in Table 9 and for the case $a > a_c$ in Table 10.

The frequency equations depend on a, b, (or $\tilde{b}$) and γ. From equations (110) [or equation (111)], b (or $\tilde{b}$) can be written as a function of a, s and γ so that the frequency equation can be written in terms of a, s, and γ only. Therefore, the roots of the frequency equations, a, depend on both s and γ. After obtaining the roots of the frequency equations in terms of a for a given s and γ, b (or $\tilde{b}$) can be found using the relationship (110) [or equation (111)]. Similarly, a can be written as a function of

TABLE 9

The frequency equations of the Timoshenko model when $a < a_c$

f-f	$\dfrac{(a^2-b^2)(a^2+b^2+\gamma^2ab-ab)(a^2+b^2-\gamma^2ab+ab)}{2ab(b^2+\gamma^2a^2)(a^2+\gamma^2b^2)} \sin a \sinh b - \cos a \cosh b + 1 = 0$
c-c	$\dfrac{(a^2-b^2)(\gamma^2a^2+\gamma^2b^2+\gamma^2ab-ab)(\gamma^2a^2+\gamma^2b^2-\gamma^2ab+ab)}{2ab(b^2+\gamma^2a^2)(a^2+\gamma^2b^2)} \sin a \sinh b - \cos a \cosh b + 1 = 0$
h-h	$\sin a \sinh b = 0$
c-f	$(a^2-b^2)\sin a \sinh b - ab\dfrac{(a^4+a^4\gamma^4+4\gamma^2a^2b^2+b^4\gamma^4+b^4)}{(b^2+\gamma^2a^2)(a^2+\gamma^2b^2)} \cos a \cosh b - 2ab = 0$

TABLE 10

The frequency equations of the Timoshenko model when $a > a_c$

f-f	$\dfrac{(a^2+\tilde{b}^2)[(a^2-\tilde{b}^2)^2+(a\tilde{b}\gamma^2-a\tilde{b})^2]}{2a\tilde{b}(-\tilde{b}^2+\gamma^2a^2)(a^2-\gamma^2\tilde{b}^2)}\sin a\sin\tilde{b}-\cos a\cos\tilde{b}+1=0$
c-c	$\dfrac{(a^2+\tilde{b}^2)[(\gamma^2a^2-\gamma^2\tilde{b}^2)^2+(\gamma^2a\tilde{b}-a\tilde{b})^2]}{2a\tilde{b}(-\tilde{b}^2+\gamma^2a^2)(a^2-\gamma^2\tilde{b}^2)}\sin a\sin\tilde{b}-\cos a\cos\tilde{b}+1=0$
h-h	$\sin a\sin\tilde{b}=0$
c-f	$(a^2+\tilde{b}^2)\sin a\sin\tilde{b}-a\tilde{b}\dfrac{(a^4+a^4\gamma^4-4\gamma^2a^2\tilde{b}^2+\tilde{b}^4\gamma^4+\tilde{b}^4)}{(-\tilde{b}^2+\gamma^2a^2)(a^2-\gamma^2\tilde{b}^2)}\cos a\cos\tilde{b}-2a\tilde{b}=0$

b (or $\tilde{b}$) using equations (110) [or equation (111)] so that the frequency equation can be written in terms of b (or $\tilde{b}$), s, and γ. The roots of the frequency equation b (or $\tilde{b}$) are found for a given s and γ. Then, the corresponding a can be found using equations (110) or (111).

The proper way to represent the roots is to make a three-dimensional plot of wave numbers as functions of s and γ. Note that the roots of the frequency equations (a and b) in the shear beam case also depend on both s and γ. However, in that case, s and γ always appear as γ/s so that we can treat γ/s as one variable. Therefore, we only needed two-dimensional plots of wave numbers as functions of γ/s. In the case of the Timoshenko beam, such a simplification cannot be made because s and γ do not always appear together. Therefore, the wave numbers are plotted for $\gamma = 2{\cdot}205$ which is a reasonable value for a thin steel hollow section.†

In order to obtain the pairs of wave numbers a_n and b_n for $a_n < a_c$ that satisfy the frequency equations, we would solve the initial-value problem given in equation (93) with the nth wave number of the Euler–Bernoulli model as an initial value to obtain a_n first, and then we would obtain b_n using equation (110) as we have done for the Rayleigh and shear models. In order to obtain the pairs of wave numbers a_n and $\tilde{b}_n$ for $a_n > a_c$, we would again solve the same initial-value problem with a_n at the transition (a_c) as the initial value instead. The value of the slenderness ratio at the nth transition is denoted as s_n so that $a_n < a_c$ or $\omega_n < \omega_c$ refers to the region where $1/s < 1/s_n$. The pairs of wave numbers are plotted in Figures 13–16. The wave number for the Euler–Bernoulli beam is included for comparison. These plots are obtained by solving an initial-value problem for the region $1/s < 1/s_n$ as done in the Rayleigh and shear beam cases. For the region $1/s > 1/s_n$, a root-finding program is used because the solution to the initial-value problem had difficulties in converging.

Note that four separate plots are shown for the hinged–hinged beam in Figure 15. Only in this case, a_n always corresponds to two values of b: a_n corresponds to

† Poisson's ratio of 0·29, outer radius of 0·16 m, and the inner radius of 0·15 m are used to obtain the shear factor $k' = 0{\cdot}53066$ using Table 3. The value of $\gamma = 2{\cdot}205$ is then obtained using equation (81).

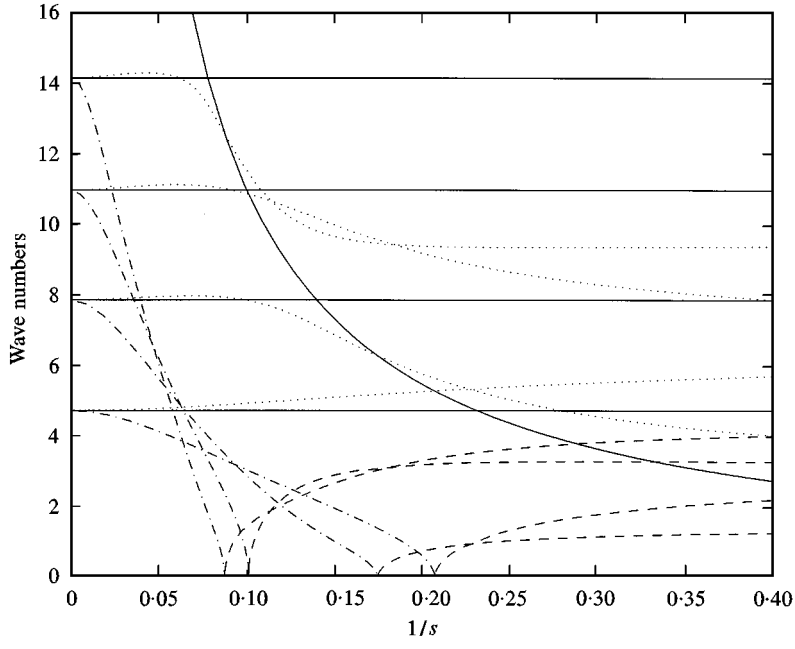

Figure 13. The first four sets of wave numbers of the free–free Timoshenko beam: —, Euler–Bernoulli; ···, a; –·–·–, b; – – –, $\tilde{b}$.

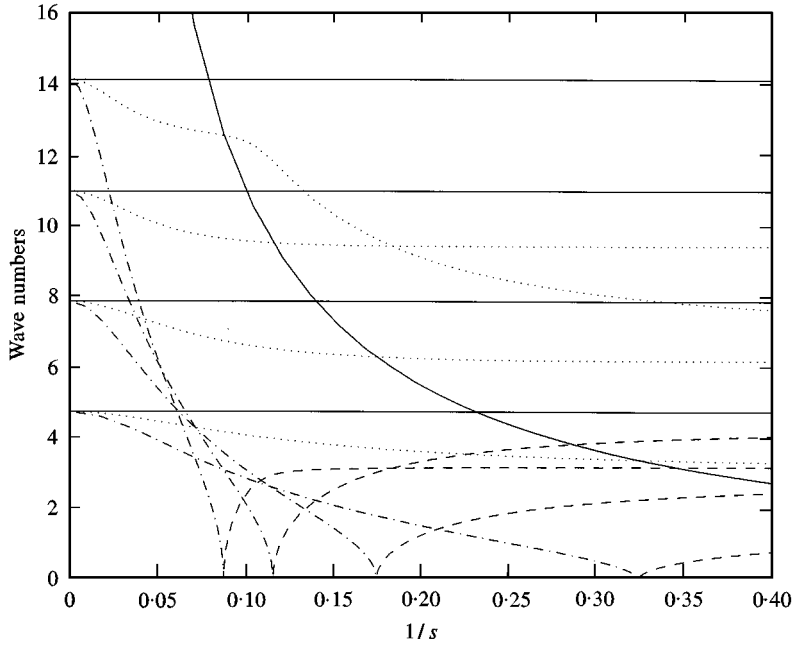

Figure 14. The first four sets of wave numbers of the clamped–clamped Timoshenko beam: —, Euler–Bernoulli; ···, a; –·–·–, b; – – –, $\tilde{b}$.

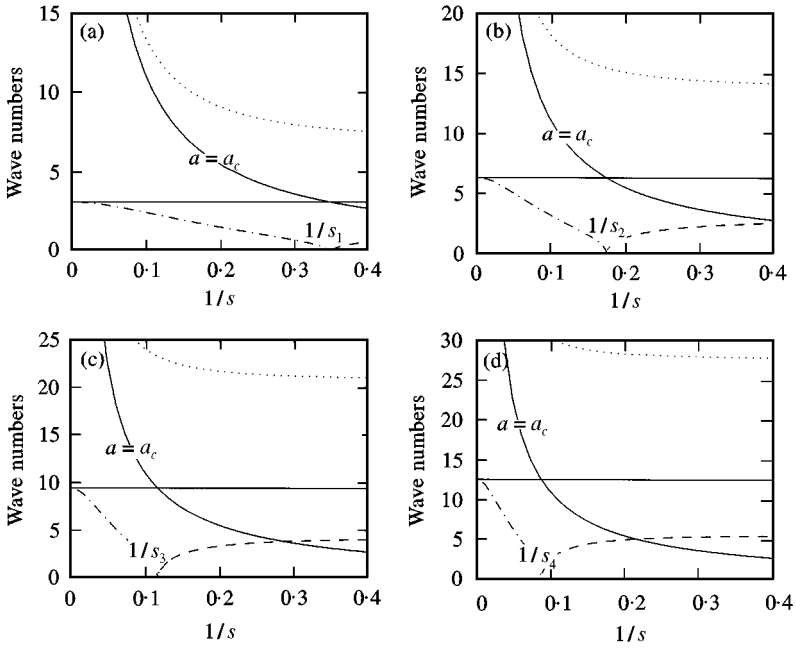

Figure 15. The first four sets of wave numbers of the hinged–hinged (or sliding–sliding) Timoshenko beam: —, Euler–Bernoulli; ⋯, a; –·–·–, b; – – –, $\tilde{b}$. (a) $n = 1$, (b) 2, (c) 3, (d) 4.

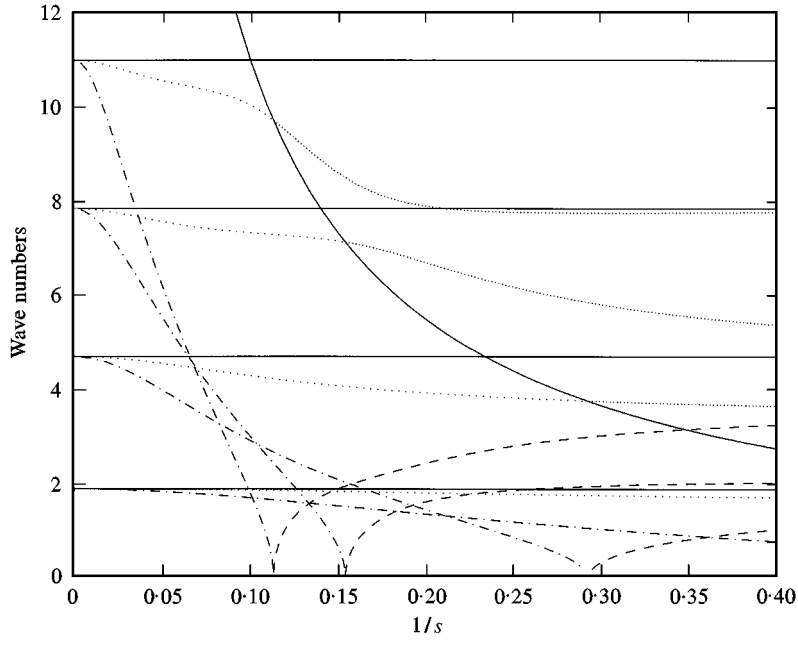

Figure 16. The first four sets of wave numbers of the clamped–free Timoshenko beam: —, Euler–Bernoulli; ⋯, a; –·–·–, b; – – –, $\tilde{b}$.

b_n and $\tilde{b}_n^{(2)}$ for $1/s < 1/s_n$ and to $\tilde{b}_n^{(1)}$ and $\tilde{b}_n^{(2)}$ for $1/s > 1/s_n$. It is important to note that each pair corresponds to a distinct natural frequency. The consequence is that there are twice as many natural frequencies in the hinged–hinged case as in other cases.

In order to explain why this is the case, let us look at the frequency equation of the hinged–hinged beam given in Table 9 or 10.

$$\sin a \sinh b = 0 \quad \text{for } a < a_c, \qquad \sin a \sin \tilde{b} = 0 \quad \text{for } a > a_c. \tag{114}$$

Note that the frequency equation is satisfied for any value of b (or $\tilde{b}$) as long as $\sin ax$ is zero (or $a_n = n\pi$ for $n = 1, 2, 3, \ldots$). When we solve for b_n (or $\tilde{b}$) that corresponds to a_n in equation (110) or (111), there are two unique expressions. When $1/s < 1/s_n$, one is real and the other is imaginary. We call the real root b_n and the imaginary root $\mathrm{i}\tilde{b}_n^{(2)}$. When $1/s > 1/s_n$, both roots are imaginary where one is $\mathrm{i}\tilde{b}_n^{(1)}$ and the other is $\mathrm{i}\tilde{b}_n^{(2)}$.

The natural frequencies that correspond to each pair can be calculated using the relation for B_1 in equations (107) and (109). The natural frequencies for the free–free, clamped–clamped, and clamped–free cases are given by

$$\omega_n^* L^* \sqrt{\rho^*/E^*} = \sqrt{\frac{a_n^2 - b_n^2}{1+\gamma^2}} \qquad \text{for } 1/s < 1/s_n$$

$$= \sqrt{\frac{a_n^2 + (\tilde{b}_n)^2}{1+\gamma^2}} \quad \text{for } 1/s > 1/s_n. \tag{115}$$

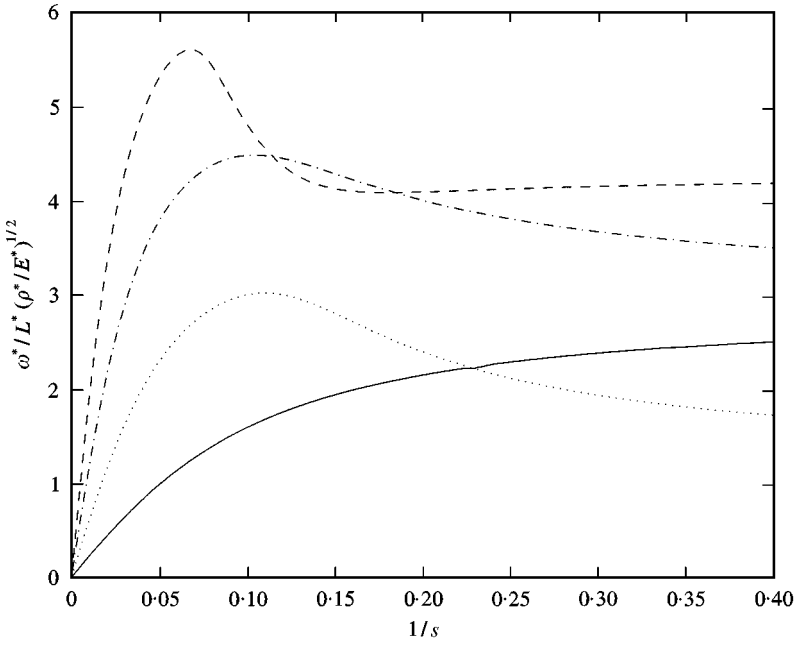

Figure 17. The frequency curves for the free–free Timoshenko beam; —, $\omega_1^* \ldots$; ⋯, $\omega_2^* \ldots$; -·-·-, $\omega_3^* \ldots$; – – –, $\omega_4^* \ldots$.

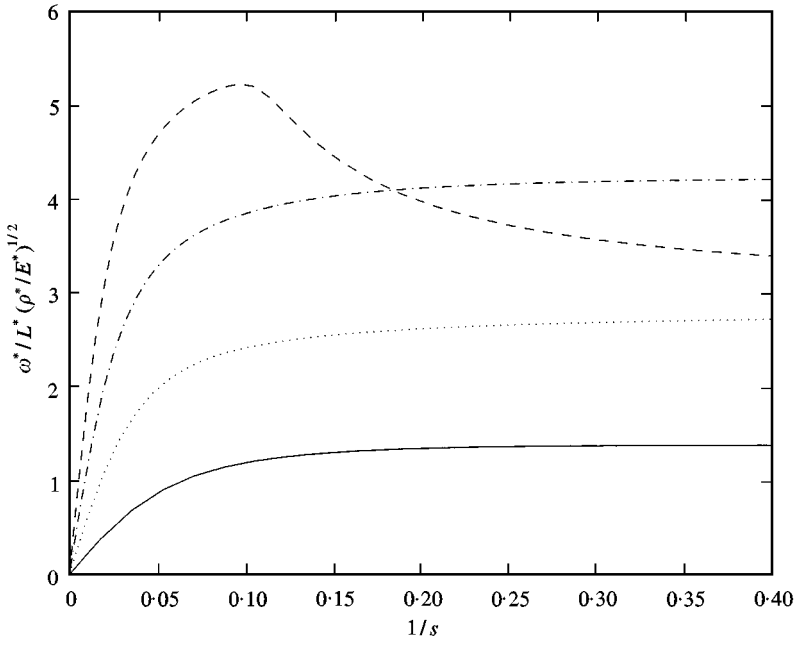

Figure 18. The frequency curves for the clamped–clamped Timoshenko beam; —, ω_1^* …; ···, ω_2^* …; -·-·-, ω_3^* …; – – –, ω_4^* ….

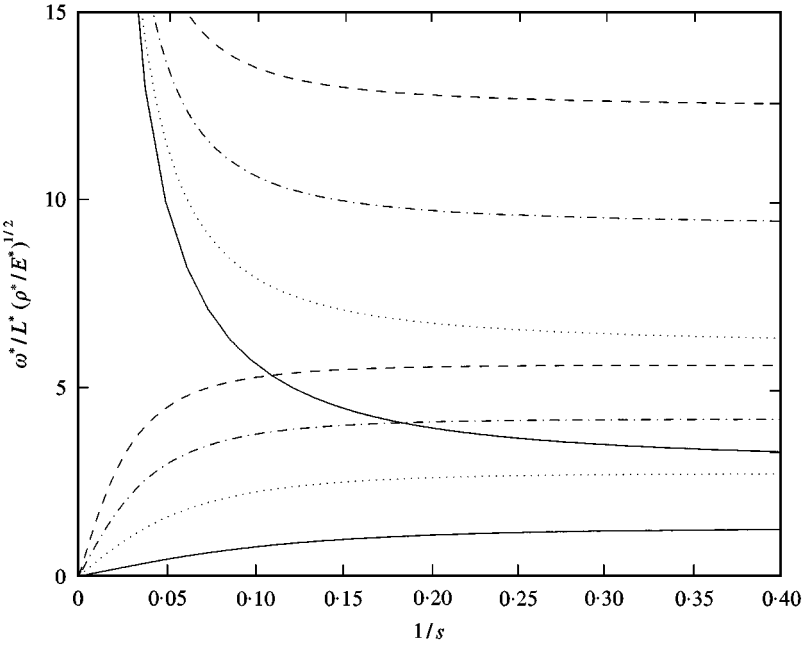

Figure 19. The frequency curves for the hinged–hinged Timoshenko beam; —, $\omega_1^{(1\text{ or }2)*}$ …; ···, $\omega_2^{(1\text{ or }2)*}$ …; -·-·-, $\omega_3^{(1\text{ or }2)*}$ …; – – –, $\omega_4^{(1\text{ or }2)*}$ ….

The quantity $\omega_n^* L^* \sqrt{\rho^*/E^*}$ is plotted as a function of $1/s$ for $\gamma = 2{\cdot}205$ in Figures 17, 18, and 20 using the values of a_n, b_n and $\tilde{b}_n$ that we know already from Figures 13, 14 and 16.

The natural frequency that corresponds to the wave number pairs (a_n, b_n) and $(a_n, \tilde{b}_n^{(1)})$ in the hinged–hinged case is denoted as $\omega_n^{*(1)}$ and is given by

$$\omega_n^{*(1)} L^* \sqrt{\rho^*/E^*} = \sqrt{\frac{a_n^2 - b_n^2}{1+\gamma^2}} \qquad \text{for } 1/s < 1/s_n$$

$$= \sqrt{\frac{a_n^2 + (\tilde{b}_n^{(1)})^2}{1+\gamma^2}} \qquad \text{for } 1/s > 1/s_n, \tag{116}$$

and the natural frequency that corresponds to the pairs of wave numbers $(a_n, \tilde{b}_n^{(2)})$ for all $1/s$ is denoted as $\omega_n^{*(2)}$ and given by

$$\omega_n^{*(2)} L^* \sqrt{\rho^*/E^*} = \sqrt{\frac{a_n^2 + (\tilde{b}_n^{(2)})^2}{1+\gamma^2}} \quad \text{for all } 1/s. \tag{117}$$

The quantities $\omega_n^{*(1,2)} L^* \sqrt{\rho^*/E^*}$ are plotted as functions of $1/s$ for $\gamma = 2{\cdot}205$ in Figure 19 using the values of a_n, b_n, $\tilde{b}_n^{(1)}$, and $\tilde{b}_n^{(2)}$ that we know from Figure 15. Note that as the slenderness ratio becomes larger $(1/s \to 0)$, the natural frequencies $\omega_n^{*(2)}$ disappear by approaching infinity. This is consistent with the other models for which $\omega_n^{*(2)}$ does not exist.

It is interesting to note that in Figures 17 and 18, curves cross each other. Thus, it is possible for a set of wave numbers with a lower index to produce a higher natural frequency. The indices of the wave numbers should not be used to gauge the order of the natural frequencies. In the other cases—the Euler–Bernoulli, Rayleigh, and shear cases—a set of wave numbers with a high index always corresponds to a higher natural frequency.

These figures can be used to obtain the wave numbers and the natural frequencies. Let us consider a clamped–free beam for $1/s = 0{\cdot}11$ and $\gamma = 2{\cdot}205$. The critical wave number a_c, obtained using equation (79), at this slenderness ratio is $10{\cdot}013$, which is slightly above a_4. Although a_5 is not plotted, we can guess that a_5 is greater than a_c. Therefore, only first four eigenfunctions will have hyperbolic terms. The sets of the wave numbers can be extracted from Figure 16. For example, a_1 in the figure is slightly less than $1{\cdot}875$, which is the wave number of the Euler–Bernoulli problem represented by the first solid line obtained from Table 5, and b_1 is slightly below a_1. Note that in order to obtain more accurate readings, the figures should be enlarged. When $\rho^* = 7830\ \text{kg/m}^3$, $L^* = 1\ \text{m}$, and $E^* = 200\ \text{GPa}$, the natural frequencies can be obtained using Figure 20. For example, from the figure the quantity $\omega_1^* L^* \sqrt{\rho^*/E^*}$ is approximately $0{\cdot}32$ which corresponds to $\omega_1^* = 1620\ \text{rad/s}$. The exact wave numbers and the natural frequencies are given by

$$(a_1, b_1) = (1{\cdot}843, 1{\cdot}655),\ \omega_1 = 1; \quad (a_2, b_2) = (4{\cdot}236, 2{\cdot}727),\ \omega_2 = 3{\cdot}991;$$

$$(a_3, b_3) = (7{\cdot}305, 2{\cdot}575),\ \omega_3 = 8{\cdot}412; \quad (a_4, b_4) = (9{\cdot}813, 0{\cdot}803),\ \omega_4 = 12{\cdot}037;$$

$$(a_5, \tilde{b}_5) = (11{\cdot}770, 2{\cdot}581),\ \omega_5 = 14{\cdot}829; \quad (a_6, \tilde{b}_6) = (13{\cdot}463, 3{\cdot}823),\ \omega_6 = 17{\cdot}224; \tag{118}$$

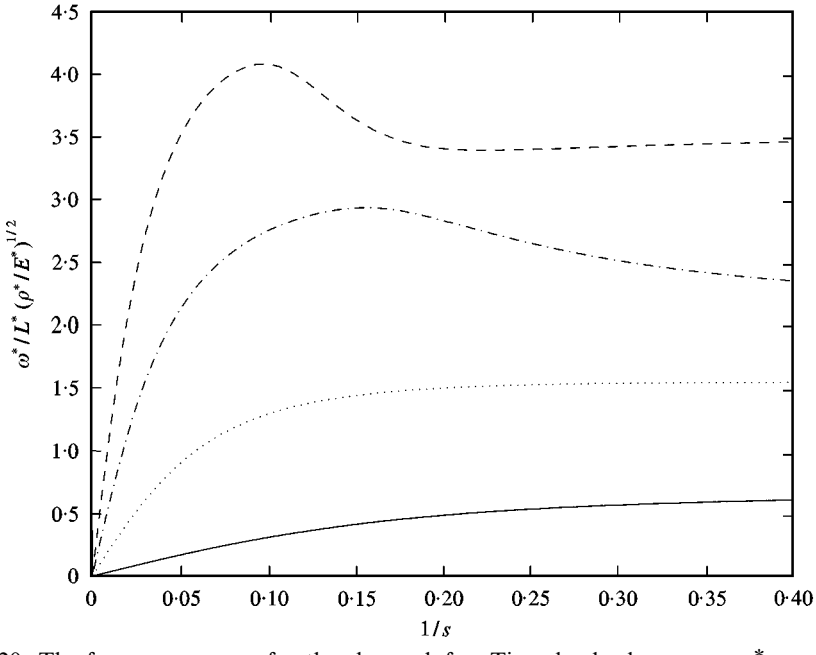

Figure 20. The frequency curves for the clamped–free Timoshenko beam; —, ω_1^* …; ⋯, ω_2^* …; –·–·–, ω_3^* …; – – –, ω_4^* ….

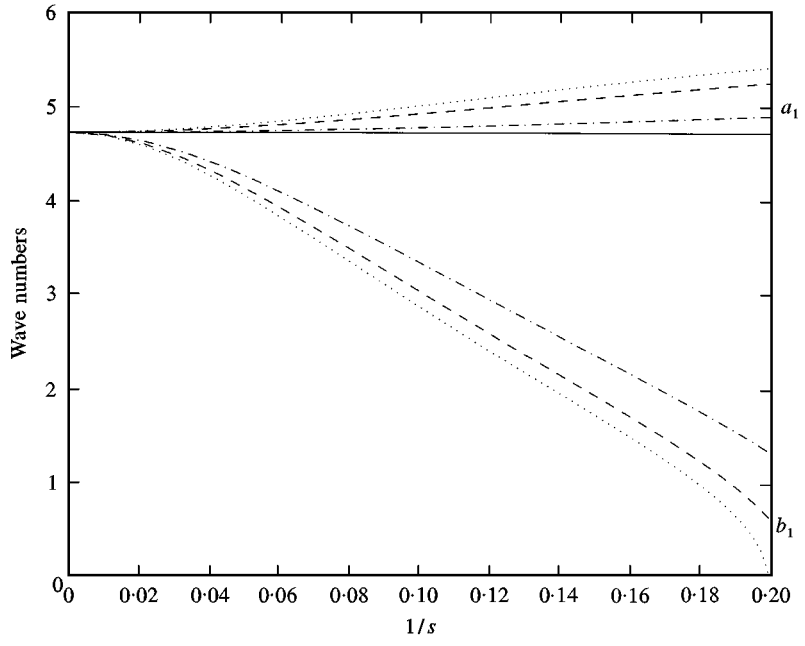

Figure 21. The first set of wave numbers of the free–free Timoshenko beam when $1/s < 1/s_1$: —, Euler–Bernoulli; ⋯, $\gamma = 2{\cdot}435$; – – –, $\gamma = 2{\cdot}205$; –·–·–, $\gamma = 1{\cdot}777$.

where the natural frequencies are non-dimensionalized by the first natural frequency $\omega_1^* = 1696$ rad/s. Note that frequencies can be read from the figure more accurately than the wave numbers.

Figure 21 shows the variation of the first pair of wave numbers (a_1, b_1) for $1/s < 1/s_1$ for the free–free Timoshenko beam shown in Figure 13. The values of γ used here are 1·7777, 2·2050 and 2·435. $\gamma = 1{\cdot}7777$ is a reasonable value for a solid circular or rectangular section, and $\gamma = 2{\cdot}435$ is a reasonable value for a thin square tube[†] with the Poisson ratio of 0·29.

4. COMPARISONS OF FOUR MODELS

So far, we obtained the wave numbers and natural frequencies of four engineering beam theories. The difference among them was the inclusion of different second order terms: rotary and shear terms. The Euler–Bernoulli model included only the first order terms, translation and bending. The Rayleigh model included the rotation, the shear model included the shear and the Timoshenko model included both rotation and shear in addition to the first order effects. In this section, we compare the relative significance of rotary and shear effects and see how it is manifested in the natural frequency and mode shapes.

The rotary effect is represented by the term ρI and the shear by $\rho/k'G$. Note that the shear term is always γ^2 times larger than the rotary term,

$$\frac{\rho}{k'G} = \frac{\rho}{k'}\frac{E^*I^*}{G^*L^{*4}} = \frac{\rho}{k'}\frac{E^*I}{G^*} = \rho I\,\frac{2(1+\nu)}{k'} = \rho I\gamma^2. \tag{119}$$

Recall that the Poisson ratio ν is a physical property that depends on the material and the shear factor k' depends on the Poisson ratio and the geometry of the cross-section. The Poisson ratio for a typical metal is about 0·3, and with this value, the shear factor for different cross-sections using, Table 3, ranges from 0·436 for the thin-walled square tube to 0·886 for the circular cross-section. Using these values, γ^2 ranges from 2·935 for the circular cross-section to 5·96 for the thin-walled square tube. We have established, for a typical material and cross-section, the shear term is roughly 3–6 times larger than the rotary term.

Now we look into circumstances under which those second order effects become important. Consider the frequency equations obtained previously in Tables 5 and 7–10. We observe that the frequency equations for the Euler–Bernoulli model depend neither on the geometrical nor the physical properties. Therefore, wave number a is independent of any properties. On the other hand, the frequency equations for the Rayleigh model are functions of a and b which are related by the slenderness ratio s. Therefore, the wave numbers a and b depend on the geometrical property s. The frequency equations for the shear and Timoshenko models depend on both s and γ. Therefore, the wave numbers depends on both geometrical and physical properties. The effects of s and/or γ on the wave numbers are shown in Figures 5–8 for the Rayleigh and shear model and in Figures 13–16 and Figure 21 for the Timoshenko model. Generally, the wave numbers deviate from those of

[†] The values of γ are calculated using the Table 3 and equation (81).

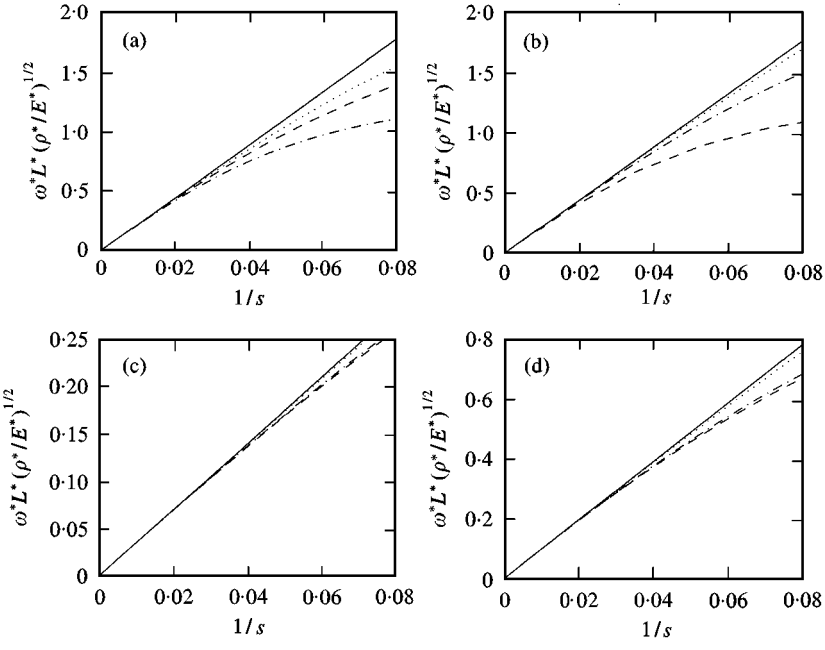

Figure 22. The frequency curves for the first natural frequency: —, Euler–Bernoulli; ···, Rayleigh; –·–·–, shear; – – –, Timoshenko. (a) Free–free beam, (b) clamped–clamped, (c) clamped–free, (d) hinged–hinged.

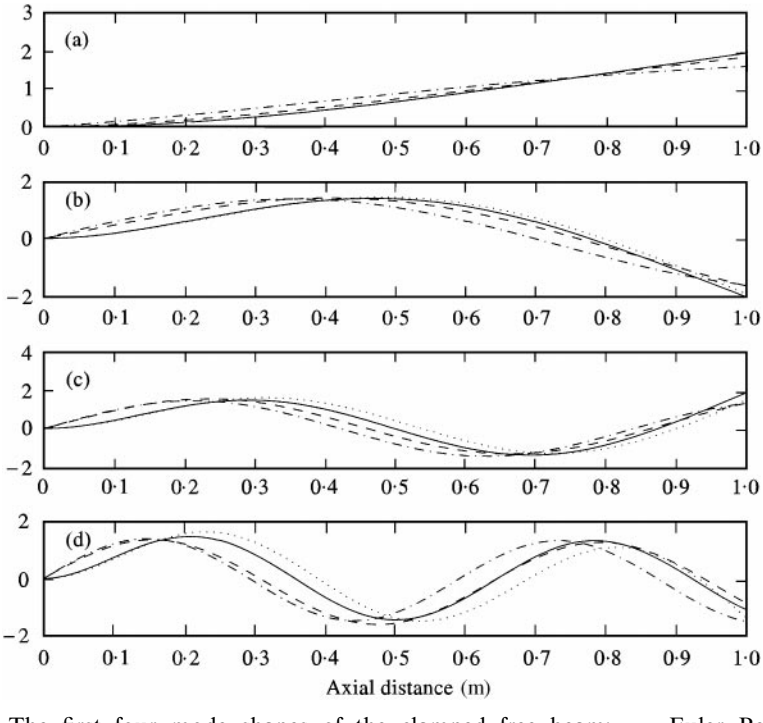

Figure 23. The first four mode shapes of the clamped–free beam: —, Euler–Bernoulli; ···, Rayleigh; –·–·–, shear; – – –, Timoshenko. (a) First mode, (b) second, (c) third, (d) fourth.

Euler–Bernoulli model as s decreases and γ increases. However, the range of γ^2 is more restricted (between 3 and 6 for a typical metal and cross-section). Therefore, the wave numbers are strong functions of the slenderness ratio.

As a numerical example, the first natural frequencies predicted by each of the four models are plotted in Figure 22. The natural frequency is multiplied by $L^*\sqrt{\rho^*/E^*}$ and $\gamma = 2{\cdot}205$ is used. The straight solid line for the Euler–Bernoulli model is obtained using equation (84). Note that the natural frequency predicted by the Euler–Bernoulli model approaches infinity as the slenderness ratio decreases whereas the natural frequencies predicted by other models level off at some point. In Figure 23, the first four mode shapes of a clamped–free beam with $s = 9{\cdot}1192$ and $\gamma = 2{\cdot}205$ are plotted. The mode shapes are normalized with respect to each other for easy comparison. Notice that the natural frequencies and mode shapes obtained using the Euler–Bernoulli and Rayleigh models are similar, and those based on the shear and Timoshenko models are similar. This confirms our result that the shear is more dominant than the rotary effects.

In summary, when the slenderness ratio is large ($s > 100$), the Euler–Bernoulli model should be used. When the slenderness ratio is small, either shear or Timoshenko model can be used.

5. THE FREE AND FORCED RESPONSE

5.1. THE ORTHOGONALITY CONDITIONS FOR THE EULER–BERNOULLI, SHEAR AND TIMOSHENKO MODELS

In order to obtain the free or forced response of the beam, we use the method of *eigenfunction expansion*. Therefore, the orthogonality conditions of the eigenfunctions have to be established for each beam model. For the models discussed so far, with the exception of the Rayleigh beam,[†] the spatial equations of the homogeneous problem, (15), (49) and (66) can be written using the operator formalism

$$L(\mathbf{W}_n) = \omega_n^2 M(\mathbf{W}_n), \tag{120}$$

where $\mathbf{W}_n$ can denote the nth eigenfunction W_n for the Euler–Bernoulli model, or the nth vector of eigenfunctions $[W_n \;\; \Psi_n]^{\mathrm{T}}$ for the shear and Timoshenko models, and corresponds to the natural frequency ω_n^2 uniquely to within an arbitrary constant [28, p. 135]. The expressions for the operators for each model are given below.

Euler–Bernoulli model:

$$L(W_n) = \frac{\mathrm{d}^4 W_n}{\mathrm{d}x^4}, \quad M(W_n) = \rho A W_n. \tag{121}$$

[†]The analysis for the Rayleigh beam is slightly different due to the mixed term in the governing differential equation. It will be discussed in detail in the next section.

Shear model:

$$L(\mathbf{W}_n) = \begin{bmatrix} k'GA\dfrac{\mathrm{d}^2}{\mathrm{d}x^2} & -k'GA\dfrac{\mathrm{d}}{\mathrm{d}x} \\ k'GA\dfrac{\mathrm{d}}{\mathrm{d}x} & \dfrac{\mathrm{d}^2}{\mathrm{d}x^2} - k'GA \end{bmatrix} \begin{bmatrix} W_n \\ \Psi_n \end{bmatrix}, \quad M(\mathbf{W}_n) = \begin{bmatrix} \rho A & 0 \\ 0 & 0 \end{bmatrix} \begin{bmatrix} W_n \\ \Psi_n \end{bmatrix}. \tag{122}$$

Timoshenko model:

$$L(\mathbf{W}_n) = \begin{bmatrix} k'GA\dfrac{\mathrm{d}^2}{\mathrm{d}x^2} & -k'GA\dfrac{\mathrm{d}}{\mathrm{d}x} \\ k'GA\dfrac{\mathrm{d}}{\mathrm{d}x} & \dfrac{\mathrm{d}^2}{\mathrm{d}x^2} - k'GA \end{bmatrix} \begin{bmatrix} W_n \\ \Psi_n \end{bmatrix}, \quad M(\mathbf{W}_n) = \begin{bmatrix} \rho A & 0 \\ 0 & \rho I \end{bmatrix} \begin{bmatrix} W_n \\ \Psi_n \end{bmatrix}. \tag{123}$$

The operators L and M are self-adjoint (with corresponding boundary conditions) if [23]

$$\int_0^1 [\mathbf{W}_n^{\mathrm{T}} L(\mathbf{W}_m) - \mathbf{W}_m^{\mathrm{T}} L(\mathbf{W}_n)]\,\mathrm{d}x = 0, \tag{124}$$

$$\int_0^1 [\mathbf{W}_n^{\mathrm{T}} M(\mathbf{W}_m) - \mathbf{W}_m^{\mathrm{T}} M(\mathbf{W}_n)]\,\mathrm{d}x = 0. \tag{125}$$

Note that the second condition, equation (125), is automatically satisfied for all three models. Using equation (120) we can write equation (124) as

$$(\omega_m^2 - \omega_n^2) \int_0^1 \mathbf{W}_n^{\mathrm{T}} M(\mathbf{W}_m)\,\mathrm{d}x = 0. \tag{126}$$

Since eigenvalues (squares of natural frequencies) are unique to the eigenfunctions, $\omega_m^2 \neq \omega_n^2$ for $m \neq n$, in order for above equation to be zero, the integral has to be zero,

$$\int_0^1 \mathbf{W}_n^{\mathrm{T}} M(\mathbf{W}_m)\,\mathrm{d}x = 0 \quad \text{for } m \neq n. \tag{127}$$

This is the orthogonality condition for the eigenfunctions. When $m = n$, we normalize the eigenfunctions by setting the integral equal to one,

$$\int_0^1 \mathbf{W}_n^{\mathrm{T}} M(\mathbf{W}_n)\,\mathrm{d}x = 1 \quad \text{for } n = 1, 2, 3, \ldots \tag{128}$$

Combining equations (127) and (128), we can write

$$\int_0^1 \mathbf{W}_n^{\mathrm{T}} M(\mathbf{W}_m)\,\mathrm{d}x = \delta_{nm}, \tag{129}$$

where δ_{nm} is the Kronecker delta.

Now we discuss which boundary conditions make the operator L self-adjoint or satisfy equation (124). The conditions can be found by substituting the expression for the operator L into equation (124) and integrating by parts. For example, for the

Euler–Bernoulli model, equation (124) becomes, substituting equation (121),

$$\int_0^1 \left[\mathbf{W}_n^{\mathrm{T}} \frac{\mathrm{d}^4 W_m}{\mathrm{d}x^4} - \mathbf{W}_m^{\mathrm{T}} \frac{\mathrm{d}^4 W_n}{\mathrm{d}x^4} \right] \mathrm{d}x = 0. \tag{130}$$

Integrating twice by parts, we obtain

$$\left(W_n \frac{\mathrm{d}^3 W_m}{\mathrm{d}x^3} - W_m \frac{\mathrm{d}^3 W_n}{\mathrm{d}x^3} \right)\Bigg|_0^1 + \left(- \frac{\mathrm{d}W_n}{\mathrm{d}x} \frac{\mathrm{d}^2 W_m}{\mathrm{d}x^2} + \frac{\mathrm{d}W_m}{\mathrm{d}x} \frac{\mathrm{d}^2 W_n}{\mathrm{d}x^2} \right)\Bigg|_0^1 = 0, \tag{131}$$

where the remaining integrals cancel each other due to symmetry. These are the conditions that have to be satisfied in order for the system to be self-adjoint and the orthogonality condition to hold. Note that the boundary conditions from the variational problem (19) satisfy this condition.

For the shear and Timoshenko models, the corresponding boundary conditions for the self-adjoint operator L are found to be

$$0 = k'GA \left[W_n \left(\frac{\mathrm{d}W_m}{\mathrm{d}x} - \Psi_m \right) - W_m \left(\frac{\mathrm{d}W_n}{\mathrm{d}x} - \Psi_n \right) \right]\Bigg|_0^1 + \left[\Psi_n \frac{\mathrm{d}\Psi_m}{\mathrm{d}x} - \Psi_m \frac{\mathrm{d}\Psi_n}{\mathrm{d}x} \right]\Bigg|_0^1, \tag{132}$$

where the boundary conditions obtained from the variational problem (61) also satisfy this condition.

Therefore, for the systems we consider, they are self-adjoint and the eigenfunctions are orthogonal to each other as given in equation (127).

5.2. THE ORTHOGONALITY CONDITIONS FOR THE RAYLEIGH MODEL

The spatial equation for the Rayleigh beam (31) can be written in the form given by equation (120) as was done for the other three models with the operators L and M given by

$$L(W_n) = \frac{\mathrm{d}^4 W_n}{\mathrm{d}x^4}, \qquad M(W_n) = \left(\rho A W_n - \rho I \frac{\mathrm{d}^2 W_n}{\mathrm{d}x^2} \right). \tag{133}$$

However, in this case, the operator M is a differential operator unlike those in the other cases. Equation (124), with the operator L substituted with equation (120) is given by

$$\int_0^1 [W_n L(W_m) - W_m L(W_n)] \, \mathrm{d}x = \int_0^1 [\omega_m^2 W_n M(W_m) - \omega_n^2 W_m M(W_n)] \, \mathrm{d}x. \tag{134}$$

Substituting the expressions for the L and M operators and integrating by parts twice, the left-hand side of equation (134) is reduced to

$$\left(W_n \frac{\mathrm{d}^3 W_m}{\mathrm{d}x^3} - W_m \frac{\mathrm{d}^3 W_n}{\mathrm{d}x^3} \right)\Bigg|_0^1 + \left(- \frac{\mathrm{d}W_n}{\mathrm{d}x} \frac{\mathrm{d}^2 W_m}{\mathrm{d}x^2} + \frac{\mathrm{d}W_m}{\mathrm{d}x} \frac{\mathrm{d}^2 W_n}{\mathrm{d}x^2} \right)\Bigg|_0^1 = 0, \tag{135}$$

where the remaining integrals cancel each other. The right-hand side of equation (134) is reduced to

$$(\omega_m^2 - \omega_n^2) \int_0^1 \left[\rho A W_m W_n + \rho I \frac{\mathrm{d}W_m}{\mathrm{d}x} \frac{\mathrm{d}W_n}{\mathrm{d}x} \right] \mathrm{d}x - \rho I \left[\omega_m^2 W_n \frac{\mathrm{d}W_m}{\mathrm{d}x} - \omega_n^2 W_m \frac{\mathrm{d}W_n}{\mathrm{d}x} \right] \Bigg|_0^1. \tag{136}$$

Combining the left- and right-hand sides equations [(135) and (136)], we obtain

$$\begin{aligned} &\left[W_n \left(\frac{\mathrm{d}^3 W_m}{\mathrm{d}x^3} + \rho I \omega_m^2 \frac{\mathrm{d}W_m}{\mathrm{d}x} \right) - W_m \left(\frac{\mathrm{d}^3 W_n}{\mathrm{d}x^3} + \rho I \omega_n^2 \frac{\mathrm{d}W_n}{\mathrm{d}x} \right) \right] \Bigg|_0^1 \\ &\quad + \left(- \frac{\mathrm{d}W_n}{\mathrm{d}x} \frac{\mathrm{d}^2 W_m}{\mathrm{d}x^2} + \frac{\mathrm{d}W_m}{\mathrm{d}x} \frac{\mathrm{d}^2 W_n}{\mathrm{d}x^2} \right) \Bigg|_0^1 \\ &= (\omega_m^2 - \omega_n^2) \int_0^1 \left[\rho A W_m W_n + \rho I \frac{\mathrm{d}W_m}{\mathrm{d}x} \frac{\mathrm{d}W_n}{\mathrm{d}x} \right] \mathrm{d}x. \end{aligned} \tag{137}$$

Let us examine the left-hand side of equation (137). Comparing with the boundary conditions from the variational problem, we find that the left-hand side vanishes [see equations (35)] so that the orthogonality condition is given by

$$\int_0^1 \left[\rho A W_m W_n + \rho I \frac{\mathrm{d}W_m}{\mathrm{d}x} \frac{\mathrm{d}W_n}{\mathrm{d}x} \right] \mathrm{d}x = \delta_{nm}. \tag{138}$$

There are other orthogonality conditions that we can obtain by manipulating equation (120), where the expressions for the operators are given by equation (133). Multiplying equation (120) by W_m and integrating over the domain ($0 \leqslant x \leqslant 1$), we obtain

$$\int_0^1 W_n \frac{\mathrm{d}^4 W_m}{\mathrm{d}x^4} \, \mathrm{d}x = \int_0^1 \omega_m^2 W_n \left(\rho A W_m - \rho I \frac{\mathrm{d}^2 W_m}{\mathrm{d}x^2} \right) \mathrm{d}x, \tag{139}$$

which can be rewritten as

$$\begin{aligned} &\int_0^1 W_n \frac{\mathrm{d}^4 W_m}{\mathrm{d}x^4} \, \mathrm{d}x + \omega_m^2 \rho I \int_0^1 \left[\frac{\mathrm{d}W_n}{\mathrm{d}x} \frac{\mathrm{d}W_m}{\mathrm{d}x} + W_n \frac{\mathrm{d}^2 W_m}{\mathrm{d}x^2} \right] \mathrm{d}x \\ &\quad = \omega_m^2 \int_0^1 \left[\rho A W_n W_m + \rho I \frac{\mathrm{d}W_n}{\mathrm{d}x} \frac{\mathrm{d}W_m}{\mathrm{d}x} \right] \mathrm{d}x, \end{aligned} \tag{140}$$

where the right-hand side equals $\omega_m^2 \delta_{nm}$ from equation (138). We integrate the left-hand side twice by parts to obtain

$$W_n \left(\frac{\mathrm{d}^3 W_m}{\mathrm{d}x^3} + \omega_m^2 \rho I \frac{\mathrm{d}W_m}{\mathrm{d}x} \right) \Bigg|_0^1 - \int_0^1 \frac{\mathrm{d}W_n}{\mathrm{d}x} \frac{\mathrm{d}^3 W_m}{\mathrm{d}x^3} \, \mathrm{d}x = \omega_m^2 \delta_{nm}. \tag{141}$$

From the boundary conditions (35), the first term vanishes and we are left with

$$- \int_0^1 \frac{\mathrm{d}W_n}{\mathrm{d}x} \frac{\mathrm{d}^3 W_m}{\mathrm{d}x^3} \, \mathrm{d}x = \omega_m^2 \delta_{nm}. \tag{142}$$

Integrating equation (142) by parts and using the boundary conditions (35) again, we obtain

$$\int_0^1 \frac{\mathrm{d}^2 W_n}{\mathrm{d}x^2} \frac{\mathrm{d}^2 W_m}{\mathrm{d}x^2}\,\mathrm{d}x = \omega_m^2 \delta_{nm}. \tag{143}$$

Therefore, we now have three orthogonality conditions given by equations (138), (142) and (143). The orthogonality condition in equation (142) will be used later.

Note that a similar procedure can be applied to the other models to obtain other orthogonality conditions.

5.3. THE FREE AND FORCED RESPONSE VIA *EIGENFUNCTION EXPANSION* OF THE EULER–BERNOULLI, SHEAR, AND TIMOSHENKO MODELS

The method of *eigenfunction expansion* assumes that the solutions $v(x,t)$ [or solutions $v(x,t)$ and $\alpha(x,t)$] to equations of motion given in equations (11), (42), (63) and the forcing function $f(x,t)$ can be represented as a summation of eigenfunctions (the spatial solution to the homogeneous problem) multiplied by functions of time that are to be determined, that is,

$$\mathbf{v}(x,t) = \sum_{n=1}^{\infty} \eta_n(t)\mathbf{W}_n(x), \qquad f(x,t) = \sum_{n=1}^{\infty} F_n(t) M(\mathbf{W}_n(x)). \tag{144, 145}$$

Note that $\mathbf{v}(x,t)$ stands for $v(x,t)$ for the Euler–Bernoulli and Rayleigh models and $[v(x,t)\ \ \alpha(x,t)]^{\mathrm{T}}$ for shear and Timoshenko models. If we know time-dependent coefficients $\eta_n(t)$, we can solve for the complete solution to the problem as follows.

The expressions for $\eta_n(t)$ can be obtained by applying the operator M to equation (144) multiplying it by $\mathbf{W}_m^{\mathrm{T}}$ and integrating over the domain. Simplifications can be made using the orthonormality conditions given in equation (129).

$$\int_0^1 \mathbf{W}_m^{\mathrm{T}} M(\mathbf{v}(x,t))\,\mathrm{d}x = \sum_{n=1}^{\infty} \eta_n(t) \int_0^1 \mathbf{W}_m^{\mathrm{T}} M(\mathbf{W}_n(x))\,\mathrm{d}x. \tag{146}$$

Therefore,

$$\eta_n(t) = \int_0^1 \mathbf{W}_m^{\mathrm{T}} M(\mathbf{v}(x,t))\,\mathrm{d}x. \tag{147}$$

Similarly, $F_m(t)$ can be found by multiplying equation (145) by $\mathbf{W}_m^{\mathrm{T}}$ and integrating over the domain,

$$F_m(t) = \int_0^1 \mathbf{W}_m^{\mathrm{T}} f(x,t)\,\mathrm{d}x. \tag{148}$$

Substituting the assumed solution (144) and the forcing function (145) into the equations of motion (11), (42), and (63), respectively, we obtain

$$\sum_{n=1}^{\infty} \frac{\mathrm{d}^2 \eta_n(t)}{\mathrm{d}t^2} M(\mathbf{W}_n(x)) + \sum_{n=1}^{\infty} \eta_n(t) L(\mathbf{W}_n(x)) = \sum_{n=1}^{\infty} F_n(t) M(\mathbf{W}_n(x)), \tag{149}$$

where the expressions for the operators M and L are given in equations (121), (122), and (123) respectively. Using equation (120), the last equation becomes

$$\sum_{n=1}^{\infty}\left[\frac{\mathrm{d}^2\eta_n(t)}{\mathrm{d}t^2}+\omega_n^2\eta_n(t)\right]M(\mathbf{W}_n(x))=\sum_{n=1}^{\infty}F_n(t)M(\mathbf{W}_n(x)). \tag{150}$$

Multiplying by $\mathbf{W}_m^{\mathrm{T}}(x)$ and integrating over the domain $(0\leqslant x\leqslant 1)$ results in

$$\frac{\mathrm{d}^2\eta_m(t)}{\mathrm{d}t^2}+\omega_m^2\eta_m(t)=F_m(t), \tag{151}$$

where the solution is given by

$$\eta_m(t)=\frac{1}{\omega_m}\int_0^t F_m(t)\sin\omega_m(t-\tau)\,\mathrm{d}\tau + \eta_m(0)\cos\omega_m t+\frac{1}{\omega_m}\frac{\mathrm{d}\eta_m}{\mathrm{d}t}\bigg|_{t=0}\sin\omega_m t. \tag{152}$$

$F_m(t)$ is given by equation (148), and $\eta_m(0)$ and $\mathrm{d}\eta_m/\mathrm{d}t|_{t=0}$ are obtained from the initial conditions, $v(x,0)$ and $\dot{v}(x,0)$, using equation (147),

$$\eta_m(0)=\int_0^1\mathbf{W}_m^{\mathrm{T}}M(\mathbf{v}(x,0))\,\mathrm{d}x,\qquad \dot{\eta}_m(0)=\int_0^1\mathbf{W}_m^{\mathrm{T}}M(\dot{\mathbf{v}}(x,0))\,\mathrm{d}x. \tag{153}$$

We now know the time-dependent coefficients $\eta_m(t)$ of equation (144) in terms of initial conditions and the forcing function. Finally, the solution is given by

$$\mathbf{v}(x,t)=\sum_{n=1}^{\infty}\eta_n(t)\mathbf{W}_n(x), \tag{154}$$

where $\eta_n(t)$ is given by equation (152).

5.4. THE FREE AND FORCED RESPONSE VIA *EIGENFUNCTION EXPANSION* OF THE RAYLEIGH MODEL

We follow a similar procedure to obtain the solution using the method of *eigenfunction expansion*. It is assumed that the solution $v(x,t)$ to the equation of motion given in equation (21) can be expanded in terms of eigenfunctions as in equation (144) or

$$v(x,t)=\sum_{n=1}^{\infty}\eta_n(t)W_n(x). \tag{155}$$

We can obtain the time-dependent coefficient $\eta_n(t)$ using the orthogonality condition given in equations (138), (142) or (143). Note that it is awkward to use the first orthogonality condition (138). Instead, we use equation (142). Taking a spatial derivative of $v(x,t)$ in equation (155), we obtain

$$\frac{\partial v(x,t)}{\partial x}=\sum_{n=1}^{\infty}\eta_n(t)\frac{\mathrm{d}W_n(x)}{\mathrm{d}x}. \tag{156}$$

Multiplying equation (156) by d^3W_m/dx^3 and integrating over the domain, we obtain

$$\eta_m(t) = -\frac{1}{\omega_m^2}\int_0^1 \frac{\partial v(x,t)}{\partial x}\frac{d^3W_m(x)}{dx^3}\,dx. \tag{157}$$

The equations of motion can be written as

$$\sum_{n=1}^{\infty}\eta_n\frac{d^4W_n}{dx^4} + \frac{d^2\eta_n}{dt^2}\left(\rho A W_n - \rho I\frac{d^2W_n}{dx^2}\right) = f(x,t). \tag{158}$$

The boundary conditions given in equation (22) can be written as

$$\frac{d^2W_n}{dx^2}\left(\delta\frac{dW_m}{dx}\right)\Bigg|_0^1 = 0, \qquad \left(\eta\frac{d^3W}{dx^3} - \rho I\frac{d^2\eta}{dt^2}\frac{dW}{dx}\right)\delta W\Bigg|_0^1 = 0. \tag{159}$$

Multiplying equation (158) by W_m and integrating over the domain $(0 < x < 1)$, we obtain

$$\sum_{n=1}^{\infty}\int_0^1\left[\eta_n\frac{d^4W_n}{dx^4} + \frac{d^2\eta_n}{dt^2}\left(\rho A W_n - \rho I\frac{d^2W_n}{dx^2}\right)\right]W_m\,dx = \int_0^1 f(x,t)\,W_m\,dx. \tag{160}$$

The left-hand side of this equation is integrated by parts,

$$\begin{aligned}\int_0^1&\left[\eta_n\frac{d^4W_n}{dx^4} + \frac{d^2\eta_n}{dt^2}\left(\rho A W_n - \rho I\frac{d^2W_n}{dx^2}\right)\right]W_m\,dx\\ &= W_m\left(\eta_n\frac{d^3W_n}{dx^3} - \frac{d^2\eta_n}{dt^2}\rho I\frac{dW_n}{dx}\right)\Bigg|_0^1 - \eta_n\frac{dW_m}{dx}\frac{d^2W_n}{dx^2}\Bigg|_0^1\\ &\quad + \int_0^1\eta_n\frac{d^2W_n}{dx^2}\frac{d^2W_m}{dx^2}\,dx + \frac{d^2\eta_n}{dt^2}\int_0^1\left[\rho A W_n W_m + \rho I\frac{dW_n}{dx}\frac{dW_m}{dx}\right]dx.\end{aligned} \tag{161}$$

Note that the terms evaluated at the boundaries disappear due to boundary conditions given in equation (159). Also, from the orthogonality conditions given in equations (138) and (143) we can simplify to

$$\int_0^1\left[\eta_n\frac{d^4W_n}{dx^4} + \frac{d^2\eta_n}{dt^2}\left(\rho A W_n - \rho I\frac{d^2W_n}{dx^2}\right)\right]W_m\,dx = \left(\eta_n\omega_n^2 + \frac{d^2\eta_n}{dt^2}\right)\delta_{nm}, \tag{162}$$

which is substituted into equation (160) so that

$$\frac{d^2\eta_m}{dt^2} + \omega_m^2\eta_m = \int_0^1 f(x,t)\,W_m\,dx. \tag{163}$$

By denoting $\int_0^1 f(x,t)\,W_m\,dx$ as $F_m(t)$, $\eta_m(t)$ is given as in equation (152). The initial conditions, $\eta_m(0)$ and $\dot{\eta}_m(0)$, can be obtained using equation (157),

$$\eta_m(0) = -\frac{1}{\omega_m^2}\int_0^1\frac{\partial v}{\partial x}\Bigg|_{(x,0)}\frac{d^3W_m(x)}{dx^3}\,dx, \qquad \dot{\eta}_m(0) = -\frac{1}{\omega_m^2}\int_0^1\frac{\partial^2 v}{\partial x\partial t}\Bigg|_{(x,0)}\frac{d^3W_m(x)}{dx^3}\,dx. \tag{164}$$

5.5. SAMPLE RESPONSES

In this section, the response of a non-slender clamped–free beam is obtained using all four models. The transverse force is given by

$$f^*(x^*, t^*) = x^* \cos 100t^*. \tag{165}$$

The beam is made of steel whose properties are given in Table 11. Using the formula given in Table 3 and the Poisson ratio given in Table 11, the shear factor for the thin round tube is $k' = 0{\cdot}53066$.

Note that the beam is not slender. Therefore, the critical wave number of the Timoshenko beam is relatively low, and the difference among the models are significant. In reality, it is hard to build a beam with such geometry and obtain reliable experimental results because the end effect will dominate the vibration. In order to avoid such problems Traill-Nash and Collar built box beams supported by diaphragms [1].

For the Euler–Bernoulli and Rayleigh models the initial displacement is given by

$$v^*(x^*, 0) = (1{\cdot}667x^{*3} - 5x^{*2})10^{-3}, \tag{166}$$

and for the shear and Timoshenko models, the initial displacement and rotation are given by

$$v^*(x^*, 0) = (2{\cdot}021x^{*3} - 6{\cdot}0635x^{*2} + 0{\cdot}7094x^*)10^{-3},$$

$$\alpha^*(x^*, 0) = (6{\cdot}0635x^{*2} - 12{\cdot}127x^*)10^{-3}. \tag{167}$$

The initial displacements are chosen so that they satisfy the boundary conditions[†] and the magnitude of the tip displacements are the same.

The natural frequencies are obtained from the frequency charts. The first four natural frequencies of the Rayleigh, shear, and Timoshenko beams are obtained previously in equations (106), (97) and (118). The natural frequencies of the Euler–Bernoulli model are obtained using the wave numbers tabulated in Table 5 and the dispersion relation given in Table 16. The natural frequencies predicted by four models are given in Table 12. The natural frequencies of the Timoshenko beam appear in pairs beyond the critical frequency because each pair of mode shapes has the same number of nodes. It may seem odd that only the Timoshenko model has more than one mode shape with same number of nodes. Experimentally, Barr (1956) [31] observed two frequencies corresponding to the same number of nodal points in the study of free–free vibration of a thick beam.

The responses are obtained using the method of *eigenfunction expansion* by summing the first eight modes of equation (144) or (155) for the Euler–Bernoulli, Rayleigh, and shear models and the first 12 modes of equation (155) for the Timoshenko model. The reason why 12 modes instead of eight are included is that by including eight modes, the Timoshenko model will be missing modes with higher number of nodes. The responses are shown in Figure 24.

[†] In fact, these initial displacements correspond to the shape of the beam when it is statically loaded by a point force at the free end.

TABLE 11

Properties of the beam

Young's modulus E^*	200 GPa [29]
Modulus of rigidity G^*	77·5 GPa
Poisson's ratio ν	0·29 [30]
Density ρ^*	7830 kg/m^3 [29]
Cross-section	round tube with $r_{inner} = 0{\cdot}15$ m, $r_{outer} = 0{\cdot}16$ m
Cross-sectional area A^*	0·0097389 m^2
Area moment of inertia I^*	0·0001171 m^2
Length L^*	1 m
Slenderness ratio $L^*\sqrt{A^*/I^*}$	9·1192
Shear factor k'	0·53066
γ	2·205

TABLE 12

Natural frequencies (rad/s)

No. of nodes	Euler–Bernoulli	Rayleigh	Shear	Timoshenko	
1	1948·62	1896·16	1797·07	—	1696·03
2	12211·80	10351·13	7231·92	—	6768·24
3	34193·39	24737·47	15150·10	—	14267·26
4	67005·41	41078·62	22842·44	—	20415·37
5	110764·74	58187·35	30509·81	25150·52	29211·86
6	165463·34	75396·16	37994·56	33792·23	38003·37
7	231101·69	92504·64	45437·80	44958·47	46401·78
8	307679·76	109447·44	52799·94	53183·33	58849·04

Notice that the response obtained using the Euler–Bernoulli and Rayleigh models are close to each other and that obtained using the shear and Timoshenko models are close to each other.

5.6. DISCUSSION ON THE SECOND FREQUENCY SPECTRUM OF THE TIMOSHENKO BEAM

Traill-Nash and Collar (1953) first claimed the existence of two separate spectra of frequencies beyond the critical frequency $\omega_c = \sqrt{k'GA/\rho I}$ for the free–free and hinged–hinged cases. That is, it is possible that two natural frequencies correspond to a single mode shape.

Both Anderson (1953) [32] and Dolph (1954) in their studies of the Timoshenko theory confirmed the result of Traill-Nash and Collar for the hinged–hinged case. Since their studies, it was generally accepted that the second spectrum existed for the hinged–hinged case. More recently, Thomas and Abbas (1975, 1977) [33, 6] showed using their finite element model that "… except for the special case of a hinged–hinged beam there is no separate second spectrum of frequencies".

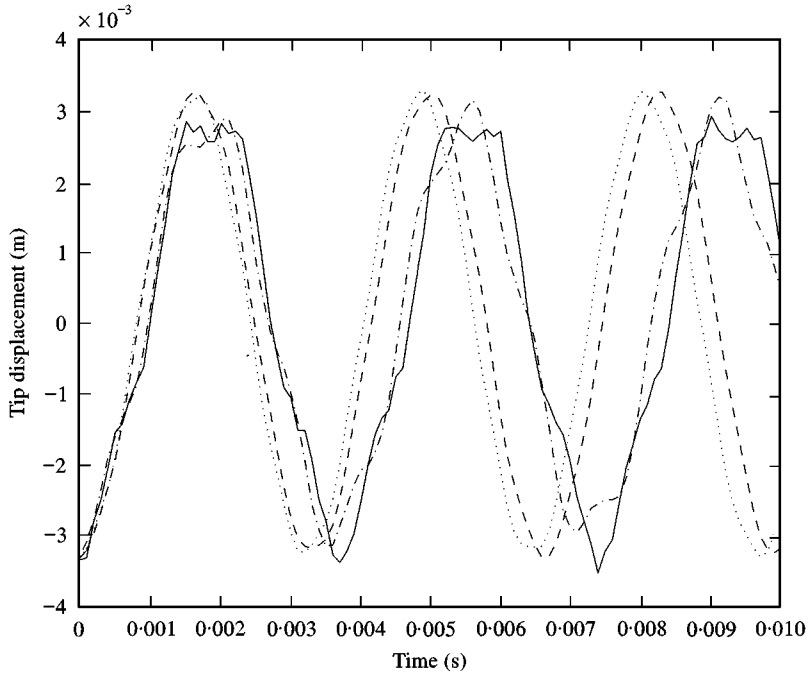

Figure 24. The response of the beam: —, Euler–Bernoulli; ···, Rayleigh; –·–·–, shear; – – –, Timoshenko.

Bhashyam and Prathap (1981) [34] also came to the same conclusion using their finite element model.

However, what previous studies neglected is that the mode shape includes both displacement and angle of rotation as a pair. If we see the displacement and the angle of rotation together, the two natural frequencies do not correspond to one mode shape. They correspond to two different mode shapes. For example, let us consider a hinged–hinged beam whose properties are given in Table 11. The natural frequencies for $1/s = 0{\cdot}11$ are shown in Figure 19, and the four lowest natural frequencies are $\omega_1^{(1)}*$, $\omega_2^{(1)}*$, $\omega_3^{(1)}*$, and $\omega_1^{(2)}*$. From Figure 15, the first natural frequency corresponds to the wave numbers $(a_1, b_1)$and the fourth natural frequency corresponds to the wave numbers $(a_1, \tilde{b}_1^{(2)})$. Note that the numerical value of a_1 is π. The spatial function in each case is given in equations (70) and (72) with coefficients related by equations (112) and (113). Upon applying boundary conditions, we find that the spatial functions are reduced to

$$\begin{bmatrix} W_1 \\ \Psi_1 \end{bmatrix} = C_1 \begin{bmatrix} \sin a_1 x \\ \dfrac{a_1^2 + \gamma^2 b_1^2}{(1+\gamma^2)a_1} \cos a_1 x \end{bmatrix}, \tag{168}$$

$$\begin{bmatrix} W_4 \\ \Psi_4 \end{bmatrix} = \tilde{C}_1 \begin{bmatrix} \sin a_1 x \\ \dfrac{a_1^2 - \gamma^2 (\tilde{b}_1^{(2)})^2}{(1+\gamma^2)a_1} \cos a_1 x \end{bmatrix}, \tag{169}$$

where the coefficients other than C_1 and $\tilde{C}_1$ are zeros. The coefficients C_1 and $\tilde{C}_1$ are then set so that the modes are normalized according to equation (129). The first and the fourth modes with corresponding natural frequencies are given by

$$\begin{bmatrix} W_1 \\ \Psi_1 \end{bmatrix} = \begin{bmatrix} 0{\cdot}158 \sin \pi x \\ 0{\cdot}323 \cos \pi x \end{bmatrix}, \quad \omega_1^{(1)*} = 4252{\cdot}56 \text{ rad/s}; \tag{170}$$

$$\begin{bmatrix} W_4 \\ \Psi_4 \end{bmatrix} = \begin{bmatrix} 0{\cdot}035 \sin \pi x \\ -1{\cdot}443 \cos \pi x \end{bmatrix}, \quad \omega_1^{(2)*} = 26881{\cdot}97 \text{ rad/s}. \tag{171}$$

Note that when the beam is vibrating at the natural frequency belonging to the "first spectrum", the amplitudes of the lateral displacement and the angle of rotation could be comparable and the bending moment ($E^*I^*\Psi$) and the shear ($k'G^*A^*(W' - \Psi)$) are in phase. When the beam is vibrating at the natural frequency belonging to the 'second spectrum', the amplitude of the angle of rotation is considerably larger than that of the lateral displacement and the bending moment and the shear are completely out of phase.

From Figure 15, we can establish inequalities given by

$$\begin{aligned} &b_n < a_n < \tilde{b}_n^{(2)} \quad \text{for } 1/s < 1/s_n \text{ and } n = 1, 2, \ldots, \\ &\tilde{b}_n^{(1)} < a_n < \tilde{b}_n^{(2)} \text{ for } 1/s > 1/s_n \text{ and } n = 1, 2, \ldots. \end{aligned} \tag{172}$$

The amplitude of the angle of rotation $(a_1^2 - \gamma^2(\tilde{b}_1^{(2)})^2)/(1 + \gamma^2)a_1$ in equation (169) is easily a large negative number. That is, the rotation of the cross-section may be large whereas the lateral deflection is minimal in the "second spectrum".

To see whether the bending moment and the shear are in phase or not, the ratios of the bending moment to the shear are obtained in both spectra,

$$\begin{aligned} \frac{\Psi_1}{W_1' - \Psi_1} \quad \frac{E^*I^*}{k'G^*A^*} &= \frac{a_1^2 + \gamma^2 b_1^2}{(a_1^2 - b_1^2)\gamma^2} \frac{E^*I^*}{k'G^*A^*}, \\ \frac{\Psi_4}{W_4' - \Psi_4} \quad \frac{E^*I^*}{k'G^*A^*} &= \frac{a_1^2 - \gamma^2(\tilde{b}_1^{(2)})^2}{\gamma^2(a_1^2 + (\tilde{b}_1^{(2)})^2)} \frac{E^*I^*}{k'G^*A^*}. \end{aligned} \tag{173}$$

Note that the first expression is always positive because a_n is always greater than b_n, and the second expression is always negative because $\tilde{b}_n^{(2)}$ is always greater than a_n. Therefore, we arrive at the conclusion that the bending moment and the shear are in phase in the "first spectrum" and completely out of phase in the "second spectrum".

Now, we can say that the two pairs of mode shapes are indeed distinct and correspond to distinct natural frequencies. There is no need to refer to them as separate frequency spectra. This has been observed by Levinson and Cooke (1982) [35] who said " … the two spectra interpretation of the predictions of Timoshenko beam theory is rather a matter of taste and not even a particularly fruitful interpretation at that".

6. SUMMARY

In this paper, we examined four approximate models for a transversely vibrating beam: the Euler–Bernoulli, Rayleigh, shear, and Timoshenko models. The equation of motion and the boundary conditions were obtained and the frequency equations for four end conditions were obtained. The solutions of the frequency equations are presented in terms of dimensionless wave numbers. Also the frequency charts are plotted so that, for a given material and geometry, the natural frequency can be obtained instantly. For each model, the orthogonality conditions are identified, and the forced response is obtained using the method of eigenfunction expansion. A numerical example is given for a non-slender beam and a brief discussion on the second frequency spectrum is included.

We found that the second order effects become more important for small s and large γ. The range of possible γ is small when compared to that of s. Therefore, the slenderness ratio alone can let us determine roughly whether or not the second order effects are important. We also found that the shear is always more dominant than the rotary effect for a given geometry and material. Therefore, either the shear or the Timoshenko model should be used for a beam with small s. The shear model may give reasonable results for less complexity.

ACKNOWLEDGMENT

This work is supported by the Office of Naval Research Grant No. N00014-94-10753. We would like to thank our program manager Dr. Thomas Swean for his interest and financial support. The first author also would like to thank Dr. Ronald Adrezin, my predecessor, for his previous works in this field [36] and his early assistance.

REFERENCES

1. R. W. Traill-Nash and A. R. Collar 1953 *Quarterly Journal of Mechanics and Applied Mathematics* **6**, 186–213. The effects of shear flexibility and rotatory inertia on the bending vibrations of beams.
2. A. E. H. Love 1927 *A Treatise on the Mathematical Theory of Elasticity*. New York: Dover Publications, Inc.
3. S. P. Timoshenko 1953 *History of Strength of Materials*. New York: Dover Publications, Inc.
4. J. W. Strutt 1877 *Theory of Sound*. London: Macmillan Publications Co., Inc.
5. R. M. Davies 1937 *Philosophical Magazine*, 563. The frequency of transverse vibration of a loaded fixed-free bar III. The effect of rotatory inertia of the bar.
6. B. A. H. Abbas and J. Thomas 1977 *Journal of Sound and Vibration* **51**, 123–137. The second frequency spectrum of Timoshenko beams.
7. S. P. Timoshenko 1921 *Philosophical Magazine*, 744. On the correction for shear of the differential equation for transverse vibrations of bars of uniform cross-section.
8. S. P. Timoshenko 1922 *Philosophical Magazine*, 125. On the transverse vibrations of bars of uniform cross-section.

9. E. T. KRUSZEWSKI 1949 *National Advisory Committee for Aeronautics*, 1909. Effects of transverse shear and rotary inertia on the natural frequencies of a uniform beam.
10. C. L. DOLPH 1954 *Quarterly of Applied Mathematics* **12**, 175–187. On the Timoshenko theory of transverse beam vibrations.
11. T. C. HUANG 1961 *Journal of Applied Mechanics*, 579–584. The effect of rotatory inertia and of shear deformation on the frequency and normal mode equations of uniform beams with simple end conditions.
12. G. HERRMANN 1955 *Journal of Applied Mechanics, Transactions of the ASME* **77**, 53–56. Forced motions of Timoshenko beam theory.
13. H. REISMANN and P. S. PAWLIK 1974 *Elastokinetics*. West Publishing Co.
14. R. D. MINDLIN and H. DERESIEWICZ 1954 *Proceedings of 2nd U.S. National Congress of Applied Mechanics*, 175–178. New York: ASME.
15. G. R. COWPER 1966 *Journal of Applied Mechanics*, 335–340. The shear coefficient in Timoshenko's beam theory.
16. G. B. SPENCE and E. J. SELDIN *Journal of Applied Physics*, 3383–3389. Sonic resonance of a bar compound torsion oscillator.
17. N. G. STEPHEN 1978 *ASME Journal of Applied Mechanics* **45**, 695–697. On the variation of Timoshenko's shear coefficient with frequency.
18. M. LEVINSON 1981 *Journal of Sound and Vibration* **77**, 440–444. Further results of a new beam theory.
19. M. LEVINSON 1981 *Journal of Sound and Vibration* **74**, 81–87. A new rectangular beam theory.
20. N. G. STEPHEN and M. LEVINSON 1979 *Journal of Sound and Vibration* **67**, 293–305. A second order beam theory.
21. H. BENAROYA 1998 *Mechanical Vibration*. Englewood Cliffs, NJ: Prentice Hall, Inc.
22. D. INMAN 1994 *Engineering Vibration*. Englewood Cliffs, NJ: Prentice Hall, Inc.
23. L. MEIROVITCH 1967 *Analytical Methods in Vibrations*. New York: Macmillan Publications Co., Inc.
24. L. MEIROVITCH 1986 *Elements of Vibration Analysis*. New York: McGraw-Hill Book Company, Inc.
25. L. MEIROVITCH 1997 *Principles and Techniques of Vibrations*. Englewood Cliffs, NJ: Prentice Hall, Inc.
26. S. S. RAO 1995 *Mechanical Vibrations*, third edition. Reading, MA, Addison-Wesley Publishing Company.
27. W. THOMSON 1993 *Theory of Vibration with Applications*, Englewood Cliffs, NJ: Prentice Hall, Inc., fourth edition.
28. R. HABERMAN 1987 *Elementary Applied Partial Differential Equations*, Englewood Cliffs, NJ: Prentice Hall, Inc., second edition.
29. E. POPOV 1990 *Engineering Mechanics of Solids*. Englewood Cliffs, NJ: Prentice Hall, Inc.
30. I. S. SOKOLNIKOFF 1956 *Mathematical Theory of Elasticity*. New York: McGraw-Hill Book Company.
31. A BARR 1956 *Proceedings of the 9th International Congress of Applied Mechanics* **7**, 448–458.
32. R. A. ANDERSON 1953 *Journal of Applied Mechanics* **75**, 504–510. Flexural vibration of uniform beams according to the Timoshenko theory.
33. J. THOMAS and B. A. H. ABBAS 1975 *Journal of Sound and Vibration* **41**, 291–299. Finite element model for dynamic analysis of Timoshenko beam.
34. G. R. BHASHYAM and G. PRATHAP 1981 *Journal of Sound and Vibration* **76**, 407–420. The second frequency spectrum of Timoshenko beam.
35. M. LEVINSON and D. W. COOKE 1982 *Journal of Sound and Vibration* **84**, 319–326. On the two frequency spectra of Timoshenko Beams.
36. R. ADREZIN 1997 *The nonlinear stochastic dynamics of tension leg platforms*. Ph.D. thesis, Rutgers, The State University of New Jersey.

APPENDIX A: NOMENCLATURE

Dimensional variables

A^*	cross-sectional area, m^2
$a^*, b^*, \tilde{b}^*$	wave numbers, 1/m
E^*	Young's modulus, N/m^2
f	transverse force normal to the structure per length, N/m
G^*	shear modulus, N/m^2
I^*	mass moment of inertia of the cross-section about the neutral axis, m^4
Q^*	shear, N
L^*	length of the beam, m
M^*	moment, N m
k^*	radius of gyration I^*/A^*, m
k'	shape factor,
KE^*	kinetic energy, $kg\,m^2/s^2$
PE^*	potential energy, $kg\,m^2/s^2$
r_i^*	ith root of the characteristic equation, 1/m
t^*	time, s
x^*	axial co-ordinate of the beam, m
$v^*(x^*, t^*)$	transverse displacement of the beam, m
$\alpha(x^*, t^*)$	angle of rotation due to bending, rad
$\beta(x^*, t^*)$	angle of rotation due to shear, rad
v	Poisson's ratio,
ρ^*	density of the beam, kg/m^3
ω_i^*	ith natural frequency of the beam, rad/s

Dimensionless variables

A	dimensionless area (A^*/L^{*2})
$a, b, \tilde{b}$	dimensionless wave numbers $(a^*L^*, b^*L^*, \tilde{b}^*L^*)$
Energy	dimensionless energy $[\text{Energy}^*L^*/(E^*I^*)]$
f	dimensionless transverse force per unit length $[f^*L^{*3}/(E^*I^*)]$
G	dimensionless shear modulus $[G^*L^{*4}/(E^*I^*)]$
I	dimensionless mass moment of inertia of the cross-section about the neutral axis (I^*/L^{*4})
Q	dimensionless shear $[Q^*L^{*2}/(E^*I^*)]$
k	dimensionless radius of gyration $(k^*/L^* = \sqrt{I/A})$
M	dimensionless moment $[M^*L^*/(E^*I^*) = \partial\alpha/\partial x]$
r_i	dimensionless ith root of the characteristic equation (r_i^*L)
s	the slenderness ratio (L^*/k^*)
t	dimensionless time $(t^*\omega_1^*)$
x	dimensionless axial co-ordinate (x^*/L^*)
v	dimensionless transverse displacement (v^*/L^*)
ρ	dimensionless density $[\rho^*(L^{*6}\omega_1^{*2})/(E^*I^*)]$
ω_n	dimensionless nth natural frequency (ω_n^*/ω_1^*)